# Proton states, anomalous conversion, and $K$-Auger spectra in $^{241}$Am from $^{241}$Cm (electron capture) and $^{245}$Bk ($\alpha$) decays*

F. T. Porter, I. Ahmad, M. S. Freedman, J. Milsted, and A. M. Friedman
*Chemistry Division, Argonne National Laboratory, Argonne, Illinois 60439*
(Received 6 May 1974)

$\gamma$ and conversion-electron spectra of mass-separated $^{241}$Cm (32.8 day) samples were measured at high resolution with Ge(Li) detectors and a magnetic $\beta$-ray spectrometer; 28 $\gamma$ rays and 76 conversion lines were identified. The multipolarities of most of the 28 transitions in $^{241}$Am were deduced. Two-parameter $\gamma$-$\gamma$ coincidences confirmed a level scheme incorporating all transitions in six rotational bands. The observed half-life of $^{241}$Cm via the decay of the 471.8 keV $\gamma$ ray was 32.8 ± 0.2 day. The $\alpha$ branching deduced from the measurements of $L_2$ and $L_3$ electron lines of the 145.5 keV transition in $^{237}$Pu was (1.0 ± 0.1)%. The $\alpha$ singles spectrum of $^{245}$Bk (5 day) decay to $^{241}$Am showed 12 $\alpha$ groups feeding the 3 lowest bands. On the basis of these measurements six single-particle states in $^{241}$Am have been identified. The ground state of $^{241}$Am is known to be $\frac{5}{2}$-[523]. The following Nilsson band-head assignments have been made: (keV, $K\pi[Nn_z\Lambda]$: 205.9, $\frac{5}{2}$+[642]; 471.8, $\frac{3}{2}$-[521]; 623.1, $\frac{1}{2}$+[400]; 652.1, $\frac{1}{2}$-[530]; and 670.2, $\frac{3}{2}$+[651]. The 266.0 keV $E1$ transition ($\frac{3}{2}$-[521] → $\frac{5}{2}$+[642]) was found to have the most highly anomalous conversion coefficients yet observed, with anomaly factors of 100–200, consistent with $E1$ penetration conversion parameter sets ($\lambda_1$, $\lambda_2$) = (18.5, 283) or (−19.3, −63); the exiting 205.9 keV $E1$ transition ($\frac{5}{2}$+[642] → $\frac{5}{2}$-[523]) shows normal $E1$ conversion. The 471.8 keV $M1$ + ~7% $E2$ transition ($\frac{3}{2}$-[521] → $\frac{5}{2}$-[523] also shows anomalous (factor of 3) conversion, with an $M1$ penetration parameter ~5.5. There is some indication of anomalously low $K$ conversion for transitions near $K$ threshold. Observed $P_1$ conversion line intensities are about twice the theoretical $P_1$ conversion coefficient predictions. Seven $KLL$- and two $KLM$-Auger electron lines were observed and the $K$-shell fluorescent yield was deduced as (96.5 ± 0.4)%.

[RADIOACTIVITY $^{241}$Cm [from $^{239}$Pu ($\alpha$, 2$n$)]; measured $T_{1/2}$, $E_\gamma$, $I_\gamma$, $X_K$, $\omega_K$, $E_{ce}$, $I_{ce}$, $e_{AKLL}$, anomalous $E1$ and $M1$ conversions, deduced penetration parameters and retardation, deduced $\alpha_{P_1}$, $\gamma\gamma$-coin, $\alpha$ branching, $^{245}$Bk [from $^{244}$Cm ($\alpha$, $p2n$)]; measured $E_\alpha$, $I_\alpha$; deduced hindrance factors. $^{241}$Am deduced levels, log$ft$ (EC), $\gamma$ multipolarity, $I$, $\pi$, 6 single-particle states. Mass-separated $^{241}$Cm. Toroidal $\beta$ spectrometer at 0.05% FWHM.]

## I. INTRODUCTION

Radiations associated with the electron capture (EC) decay of $^{241}$Cm were first investigated by Asaro *et al.*[1]; they observed two $\gamma$ rays with energies 470 and 600 keV. On the basis of coincidence measurements levels at 470 and 600 keV were postulated in $^{241}$Am. However, because of lack of detailed information these states could not be given Nilsson-state[2] assignments.

The $\alpha$ decay of $^{245}$Bk was studied by Ahmad[3] who identified 11 $\alpha$ groups populating three rotational bands in $^{241}$Am. On the basis of $\gamma$-ray multipolarities the levels at 207 and 475 keV were assigned to the $\frac{5}{2}$+[642] and $\frac{3}{2}$-[521] proton orbitals, respectively. The present study was undertaken with the aim of identifying the levels around 600 keV in $^{241}$Am and deducing the reduced electron capture half-lives to the observed single-particle states. The EC decay of $^{241}$Cm was investigated with high-resolution Ge(Li) $\gamma$ and magnetic electron spectrometry and five new levels and three new single-particle states in $^{241}$Am were identified. The $^{245}$Bk $\alpha$ decay was studied by $\alpha$-particle spectroscopy with results in agreement with Ahmad's.[3]

## II. SOURCE PREPARATION

The $^{241}$Cm samples for the present measurements were prepared by irradiating $^{239}$Pu with 40 MeV $\alpha$ particles in the Argonne 60-in. cyclotron using the external beam defocused to a 1 × 10-cm strip. The 100-$\mu$ thick Pu target (same dimensions) was in the form of a Pu-Al alloy (98.2% Pu) of isotopic composition 95% $^{239}$Pu, ~4% $^{240}$Pu, and ~1% $^{241}$Pu. The alloy foil was welded onto an aluminum plate which was water cooled during the irradiation period. Each irradiation was of 5 days duration with a beam intensity of 40–80 $\mu$A.

After irradiation the target was allowed to de-

cay for several days before the Pu-Al alloy was dissolved in a mixture of NaOH and $NaNO_2$. This procedure dissolved the aluminum and precipitated the plutonium, americium, and curium as a slurry. The slurry was dissolved in hydrochloric acid and the Cm-Am fraction was separated from Pu and fission products by a series of standard ion-exchange resin columns. Cm and Am were separated from each other by adsorption on a cation exchange resin column followed by elution with ammonium $\alpha$-hydroxy isobutyrate[4]; two such columns were required to obtain a curium sample free from $^{241}$Am. Thin samples of $^{241}$Cm for electron and $\gamma$ spectroscopy were prepared by the deposition of 100 eV $^{241}$Cm ions through a 1-mm aperture mask onto 5-mg/cm$^2$ aluminum foils in the Argonne electromagnetic isotope separator.[5]

The $^{245}$Bk sample for $\alpha$ spectroscopy was prepared by the irradiation of a $^{244}$Cm target with 43 MeV $\alpha$ particles. The Bk activity was isolated and purified by the procedure described in Ref. 6.

## III. EXPERIMENT

### A. $\gamma$-ray spectroscopy

Several $\gamma$-singles spectra of mass-separated $^{241}$Cm samples were measured with a 1-cm$^3$ planar Ge(Li) detector and a 25-cm$^3$ coaxial Ge(Li) detector. The low energy portion of a spectrum of mass-separated $^{241}$Cm measured with a 2-cm$^2$ × 5-mm planar Ge(Li) detector is shown in Fig. 1. This spectrometer had a 24-mg/cm$^2$ beryllium window and a resolution [full width at half-maximum (FWHM)] of 600 eV at 100 keV $\gamma$-ray energy. The gain of the counting system was controlled with a digital gain stabilizer. Energy standards[7] used were transitions in the decay of $^{182}$Ta, $^{57}$Co, and $^{139}$Ce. In particular the Am $K\ \alpha_2$ and Am $K\ \alpha_1$ energies were measured with respect to the 100.105 ± 0.001 keV $\gamma$ ray of $^{182}$Ta; the source and the standard were counted simultaneously. Energies and intensities of $\gamma$ rays and $K$ x rays determined with this detector are given in Table I. The present values of 102.024 ± 0.020 and 106.465 ± 0.020 keV for the $K\ \alpha_2$ and $K\ \alpha_1$ x rays agree within quoted errors with crystal diffraction values[8] of 102.041 ± 0.006 and 106.484 ± 0.006 keV, and with conversion line energy differences from the electron spectroscopy reported here, 102.030 ± 0.005 and 106.472 ± 0.007 keV.

High energy $\gamma$ rays were identified in spectra measured with a 25-cm$^3$ Ge(Li) spectrometer. Figure 2 shows the $^{241}$Cm spectrum obtained by placing a mass-separated $^{241}$Cm sample ~10 cm

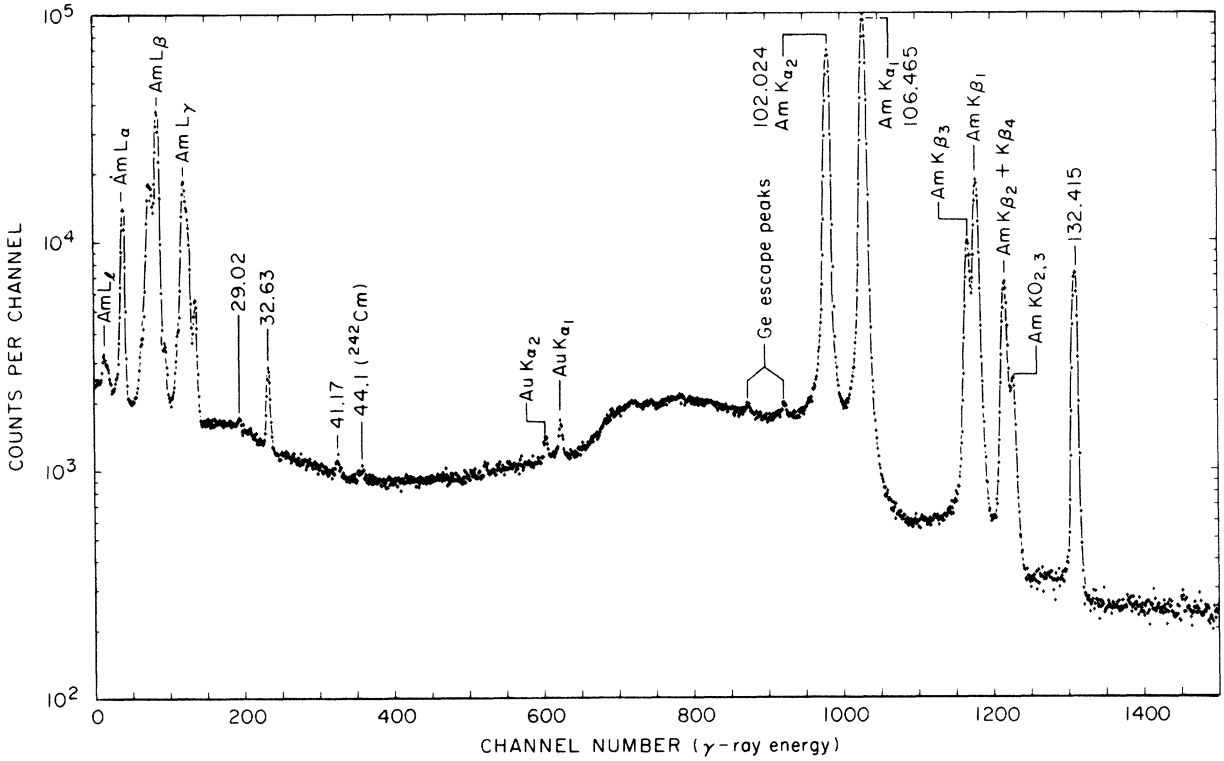


FIG. 1. $\gamma$-ray spectrum of mass-separated $^{241}$Cm sample measured through 350-mg/cm$^2$ Al absorber with 2-cm$^2$ × 0.5-cm Ge(Li) detector. Source placed ~3 cm from detector end cap. Au $K$ x rays originate from fluorescence of gold electrode on detector. Counting time was 21 h. Observed channel number equals abscissa value plus 150.

TABLE I. $^{241}$Cm $\gamma$ rays and $K$ x rays.

| Energy (keV) | Photon intensity (% per EC decay) | Transition (initial → final level) | Energy (keV) | Photon intensity (% per EC decay) | Transition (initial → final level) |
|---|---|---|---|---|---|
| 29.02 ± 0.05 | 0.03 ± 0.006 | 652.1 → 623.1 | 298.5 ± 0.3 | 0.08 ± 0.02 | 504.4 → 205.9 |
| 32.63 ± 0.03 | 0.21 ± 0.03 | 504.4 → 471.8 | 410.8 ± 0.1 | 0.087 ± 0.009 | 504.4 → 93.6 |
| 41.17 ± 0.05 | 0.017 ± 0.004 | 41.2 → 0 | 417.3 ± 0.1 | 0.66 ± 0.04 | 623.1 → 205.9 |
| 102.024 ± 0.020 | 23.2 ± 1.4 | Am $K\ \alpha_2$ | 430 ± 1 | ~0.04 | 636.8 → 205.9 |
| 106.465 ± 0.020 | 36.8 ± 2.1 | Am $K\ \alpha_1$ | 430.7 ± 0.1 | 4.1 ± 0.22 | 471.8 → 41.2 |
| 119.255 ± 0.030 | 4.5 } 13.9 ± 0.9 | Am $K\ \beta_3$ | 447.3 ± 0.2 | 0.12 ± 0.015 | 653.2 → 205.9 |
| 120.274 ± 0.030 | 9.4 } | Am $K\ \beta_1$ | 463.3 ± 0.1 | 1.24 ± 0.08 | 504.4 → 41.2 |
| 123.750 ± 0.030 | 3.8 } 4.9 ± 0.3 | Am $K\ \beta_2 + K\beta_4$ | 464.4 ± 0.3 [a] | 0.086 ± 0.014 | 670.2 → 205.9 |
| 124.816 ± 0.030 | 1.1 } | Am $KO_{2,3}$ | 471.8 ± 0.1 | 72 ± 3 | 471.8 → 0 |
| 132.415 ± 0.030 | 3.9 ± 0.2 | 636.8 → 504.4 | 504.4 ± 0.1 | 0.60 ± 0.04 | 504.4 → 0 |
| 151.4 ± 0.4 [a] | ~0.02 | 623.1 → 471.8 | 595.8 ± 0.3 | 0.015 ± 0.003 | 636.8 → 41.2 |
| 164.8 ± 0.2 [a] | 0.44 ± 0.09 | 205.9 → 41.2 | 623.1 ± 0.3 | 0.012 ± 0.003 | 623.1 → 0 |
| 165.05 ± 0.04 | 3.0 ± 0.2 | 636.8 → 471.8 | 636.8 ± 0.1 | 1.55 ± 0.11 | 636.8 → 0 |
| 180.30 ± 0.04 | 0.48 ± 0.04 | 652.1 → 471.8 | 652.1 ± 0.4 | 0.04 ± 0.01 | 652.1 → 0 |
| 205.87 ± 0.04 | 2.7 ± 0.15 | 205.9 → 0 | 653.2 ± 0.2 | 0.15 ± 0.01 | 653.2 → 0 |
| 265.95 ± 0.08 | 0.40 ± 0.04 | 471.8 → 205.9 | 670.2 ± 0.2 | 0.58 ± 0.04 | 670.2 → 0 |

[a] Observed only in $\gamma$-$\gamma$ coincidence.

away from the detector end cap. A $\gamma$-ray spectrum measured with a set of absorbers (0.7-g/cm$^2$ Pb, 1.0-g/cm$^2$ Cd, 0.7-g/cm$^2$ Cu, and 0.5-g/cm$^2$ Al) interposed between the source and the detector is displayed in Fig. 3. The absorbers were used to reduce summing-effect interference from low energy $\gamma$ rays and $K$ x rays. The peaks marked B in Fig. 3 are due to the background. Energies and intensities of $\gamma$ rays thus determined are included in Table I. The intensities expressed in photons per 100 $^{241}$Cm EC decays were obtained by equating the total $\gamma$-ray and conversion-electron intensities populating the ground-state band to 100%. Electron and photon intensities were related to each other through the theoretical absolute $L$-conversion coefficients of the 132.4, 165.0 and the $K$ and $L$ coefficients of the 205.9 keV transitions, based on the multipolarity mixtures obtained from $L$, $M$, and $N$ conversion ratios in the first two predominantly $M1$ transitions, and on the assumption that the 205.9 keV transition is pure $E1$. An average of these normalization factors was used. Its uncertainty based on deviations of the individual normalization factors from the mean was ~5%. The 132.4 and 165.0 keV $K$ lines were not used in this relative normalization because of disparities in their apparent conversion coefficients; see discussion in Sec. IV C.

### B. Conversion-electron spectroscopy

The conversion-electron lines associated with the $^{241}$Cm decay were measured with the Argonne toroidal-field spectrometers[9] operated in tandem. The spectra were run with a 1-mm-diam source and an exit aperture of 1.5 mm diameter. Under these conditions the instrument had a resolution (FWHM, momentum) of 0.05% and a transmission of 4.4% of $4\pi$. The source containing ~$5 \times 10^5$ dis/min had a mass density, as estimated from the isotope separator beam current and separation time, of <1 $\mu$g/cm$^2$.

Line positions were determined by extrapolating the median at various heights to the line peak. Spectrometer calibration was based on the $K$-conversion line of the 122.060 ± 0.004 keV transition in $^{57}$Fe (Ref. 10). Atomic electron binding energies in Am for $K$, $L_{1-3}$, $M_{1-3}$, $N_{1-3}$, $O_{1-3}$, and $P_1$ shells in the (oxidized) source were derived from the observed line energies and decay scheme considerations, with errors in the range of 3–6 eV. This derivation of binding energies will be published elsewhere.

Line areas on a counting rate vs momentum plot were graphically integrated for certain well-defined lines and the ratio of the line area to peak height was plotted as a function of the line momentum. Separate curves were generated for $K$ and for $L$, $M$, ... lines to allow for the large differences in the natural width contributions to line breadth. The peak heights for weaker or incompletely resolved lines were thus converted to peak areas. These areas, corrected for decay and detector efficiency as a function of electron energy, gave the electron intensities listed in Table II in percent per EC decay. The errors in intensities include contributions from line area and decay constant uncertainties but not those of detector efficiency, which may enhance low energy intensity errors significantly. The efficiency of the de-

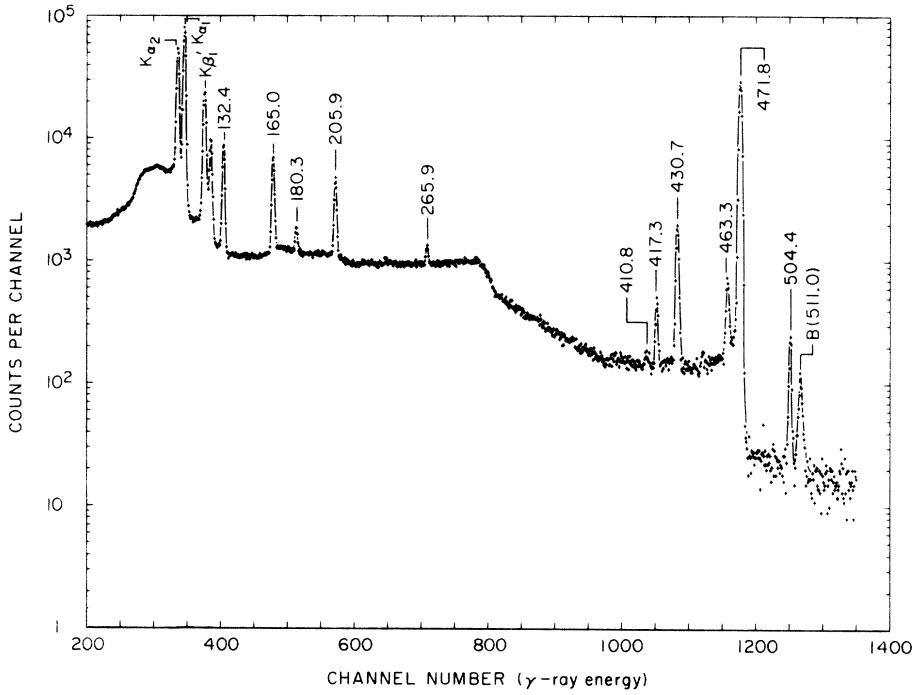


FIG. 2. $^{241}$Cm $\gamma$-ray spectrum measured through 450-mg/cm$^2$ Al with 25-cm$^3$ coaxial Ge(Li) detector. Source placed ~ 10 cm from detector end cap. Counting time 15 h. Peak B (511.0) is background radiation.

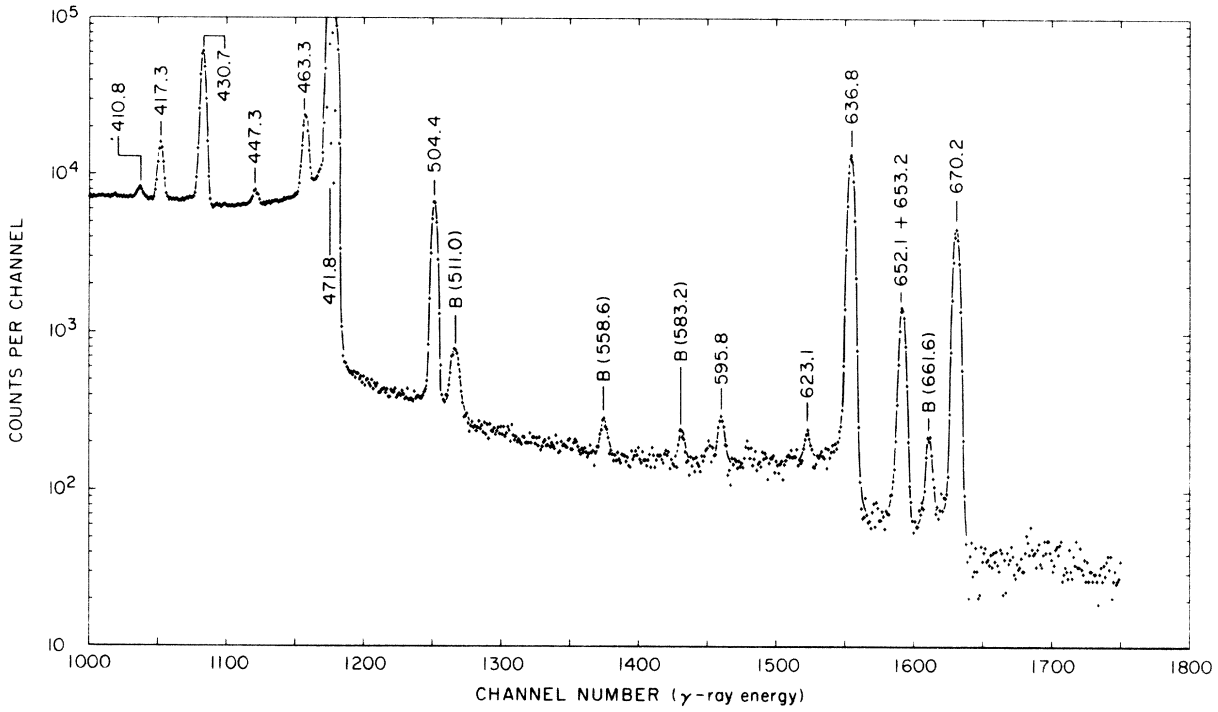


FIG. 3. High-energy portion of $^{241}$Cm (mass-separated) $\gamma$-ray spectrum measured with 25-cm$^3$ Ge(Li) detector. A set of Pb, Cd, Cu, and Al absorbers absorbed low energy $\gamma$ rays and Am $K$ x rays. Counting time was 63 h. Peaks labeled B are background radiation.

TABLE II. Transitions in $^{241}$Am following electron capture in $^{241}$Cm: internal conversion electrons and $\gamma$ rays.

| Transition energy [keV(±eV)] [a] (initial → final state) | Shell [c] | Electron energy [keV(±eV)] [d] | Transition energy [keV(±eV)] [e] | Intensity [b] (% per $^{241}$Cm EC) | Multipolarity: mixing derived from: |
|---|---|---|---|---|---|
| 15.2276(2) | $M_1$ | 9.0919(0.9) | 15.2279(2.5) | 15.3 ± 0.7 | (0.10 ± 0.02)% $E2$ |
| (652.1 → 636.9) | $M_2$ | 9.4813(0.9) | 15.2283(2.7) | 3.0 ± 0.3 | +99.9% $M1$ |
| | $M_3$ | 10.5226(1.8) | 15.229(4) | 1.0 ± 0.1 | $M_1/M_2, M_1/M_3$ |
| | $N_1$ | 13.6047(1.0) | 15.2277(2.9) | 4.5 [f] | |
| | $N_2$ | 13.782(2) | 15.228(4) | 0.86 [f] | |
| | $N_3$ | 14.056(2) | 15.224(4) | 0.51 ± 0.15 | |
| | $O_1$ | 14.853(16) | 15.226(16) | 1.06 [f] | |
| | $O_2$ | 14.928(5) | 15.231(7) | 0.21 ± 0.06 | |
| | $P_1$ | 15.172(3) | 15.224(6) | 0.46 ± 0.05 | |
| | Other | | | 0.16 | |
| | $\gamma$ | | | 0.056 [f] | |
| | | | | 27.1 ± 0.9 | |
| 29.02(50) | $e^-$ | | | 0.11 | |
| (652.1 → 623.1) | $\gamma$ | | 29.02(50) | 0.03 ± 0.006 | $E1$ scheme |
| | | | | 0.14 ± 0.03 | |
| 32.6386(3) | $L_1$ | 8.8288(0.8) | 32.640(4) | 24.7 ± 1.3 | (1.5 ± 0.2)% $E2$ |
| (504.4 → 471.8) | $L_2$ | 9.6840(0.9) | 32.639(4) | 7.9 ± 0.4 | +98.5% $M1$ |
| | $L_3$ | 14.1248(1.0) | 32.638(4) | 4.9 ± 0.2 | $L_1/L_2, L_1/L_3$, |
| | $M_1$ | 26.503(1) | 32.639(3) | 5.6 ± 0.3 | $M_1/M_2, M_1/M_3$, |
| | $M_2$ | 26.890(2) | 32.637(4) | 1.50 ± 0.18 | $N_1/N_2, N_1/N_3$, |
| | $M_3$ | 27.934(4) | 32.640(6) | 0.94 ± 0.14 | $\alpha_{L_1}, \alpha_{M_1}, \alpha_{N_1}$ |
| | $M_4$ | | | ≤0.04 | |
| | $M_5$ | | | ≤0.03 | |
| | $N_1$ | 31.016(2) | 32.639(4) | 1.71 ± 0.08 | |
| | $N_2$ | 31.193(3) | 32.639(5) | 0.47 ± 0.04 | |
| | $N_3$ | 31.471(3) | 32.639(5) | 0.28 ± 0.04 | |
| | $N_4$ | | | ≤0.08 | |
| | $N_5$ | | | ≤0.08 | |
| | $O_1$ | 32.266(3) | 32.639(5) | 0.39 ± 0.02 | |
| | $O_2$ | 32.332(5) | 32.635(7) | 0.16 ± 0.02 | |
| | $O_3$ | 32.410(5) | 32.635(8) | 0.08 ± 0.02 | |
| | $P_1$ | 32.586(5) | 32.638(8) | 0.12 ± 0.02 | |
| | Other | | | 0.08 | |
| | $\gamma$ | | 32.63(30) | 0.21 ± 0.03 | |
| | | | | 49.0 ± 1.4 | |
| 41.176(3) | $L_1$ | 17.366(2) | 41.177(4) | 0.90 ± 0.13 | (16 ± 3)% $E2$ |
| (41.18 → 0) | $L_2$ | 18.2213(1.2) | 41.176(4) | 1.76 ± 0.16 | +84% $M1$ |
| | $L_3$ | 22.6632(0.4) | 41.176(4) | 1.20 ± 0.06 | $L_1/L_2, L_1/L_3$, |
| | $M_1$ | 35.044(15) | 41.180(15) | 0.16 ± 0.05 | $M_1/M_2, \alpha_{L_3}$ |
| | $M_2$ | 35.432(12) | 41.179(13) | 0.42 ± 0.05 | |
| | Other | | | 0.72 | |
| | $\gamma$ | | 41.17(50) | 0.017 ± 0.004 | |
| | | | | 5.2 ± 0.2 | |
| 132.413(7) | $K$ | 7.424(4) | 132.409(9) | 33.0 ± 1.6 | (0.4 ± 0.2)% $E2$ |
| (636.8 → 504.4) | $L_1$ | 108.5975(1.3) | 132.408(7) | 7.7 ± 0.4 | +99.6% $M1$ |
| | $L_2$ | 109.4559(1.3) | 132.411(7) | 1.00 ± 0.07 | $L_1/L_3, L_1/L_2$, |
| | $L_3$ | 113.903(13) | 132.416(15) | 0.056 ± 0.011 | $M_1/M_2, N_1/N_2$ |
| | $M_1$ | 126.274(6) | 132.410(10) | 1.85 ± 0.08 | |
| | $M_2$ | 126.674(11) | 132.421(13) | 0.27 ± 0.09 | |
| | $N_1$ | 130.787(6) | 132.410(10) | 0.56 ± 0.03 | |
| | $N_2$ | 130.984(14) | 132.430(16) | 0.082 ± 0.022 | |
| | $N_3$ | | | ≤0.02 | |
| | $O_1$ | 132.039(6) | 132.412(10) | 0.153 ± 0.014 | |
| | $O_{2,3}$ | | | ≤0.02 | |
| | $P_1$ | 132.388(14) | 132.440(16) | 0.054 ± 0.022 | |

TABLE II *(Continued)*

| Transition energy [keV(±eV)] [a] (initial → final state) | Shell [c] | Electron energy [keV(±eV)] [d] | Transition energy [keV(±eV)] [e] | Intensity [b] (% per $^{241}$Cm EC) | Multipolarity: mixing derived from: |
|---|---|---|---|---|---|
| | Other | | | 0.04 | |
| | $\gamma$ | | 132.415(30) | 3.9 ± 0.2 | |
| | | | | 48.7 ± 1.7 | |
| 147.67(27) | $K$ | | | ≤0.33 | |
| (652.1 → 504.4) | $L_1$ | | | ≤0.01 | $E2$ scheme |
| | $L_2$ | 124.714(27) | 147.667(27) | 0.027 ± 0.010 | |
| | $L_3$ | | | ≤0.011 | |
| | Other | | | 0.036 | |
| | $\gamma$ | | | 0.02 [f] | |
| | | | | 0.083 ± 0.032 | |
| 151.4(400) | $e^-$ | | | ... | $E1$ scheme |
| (623.1 → 471.8) | $\gamma$ | | 151.4(400) | ~0.02 | |
| | | | | ~0.02 | |
| 164.8(200) | $e^-$ | | | 0.07 | |
| (205.9 → 41.18) | $\gamma$ | | 164.8(200) | 0.44 ± 0.09 | $E1$ scheme |
| | | | | 0.51 ± 0.10 | |
| 165.049(8) | $K$ | 40.061(2) | 165.046(9) | 14.0 ± 0.7 | (5.7 ± 0.9)% $E2$ |
| (636.8 → 471.8) | $L_1$ | 141.237(3) | 165.048(8) | 2.95 ± 0.15 | +94.3% $M1$ |
| | $L_2$ | 142.091(3) | 165.046(8) | 0.49 ± 0.03 | $L_1/L_2, L_1/L_3$, |
| | $L_3$ | 146.536(20) | 165.049(20) | 0.068 ± 0.019 | $M_1/M_2, N_1/N_2$ |
| | $M_1$ | 158.917(6) | 165.053(10) | 0.75 ± 0.06 | |
| | $M_2$ | 159.306(21) | 165.053(22) | 0.14 ± 0.06 | |
| | $N_1$ | 163.426(14) | 165.049(16) | 0.20 ± 0.02 | |
| | $N_2$ | 163.643(44) | 165.089(44) | 0.044 ± 0.009 | |
| | $O_1$ | 164.680(29) | 165.053(30) | 0.07 ± 0.02 | |
| | $P_1$ | | | ≤0.04 | |
| | Other | | | 0.05 | |
| | $\gamma$ | | 165.05(40) | 3.0 ± 0.2 | |
| | | | | 21.8 ± 0.8 | |
| 180.277(8) | $K$ | 55.293(2) | 180.278(11) | 2.09 ± 0.11 | $M1$ |
| (652.1 → 471.8) | $L_1$ | 165.464(2) | 180.275(9) | 0.42 ± 0.02 | ($E2 \leq 7\%$) |
| | $M_1$ | 174.146(21) | 180.282(23) | 0.104 ± 0.015 | $\alpha_K, \alpha_{L_1}$, |
| | Other | | | 0.12 | $\alpha_{M_1}$ |
| | $\gamma$ | | 180.30(40) | 0.48 ± 0.04 | |
| | | | | 3.21 ± 0.12 | |
| 205.879(13) | $K$ | 80.901(12) | 205.886(16) | 0.22 ± 0.02 | $E1$ |
| (205.9 → 0) | $L_1$ | 182.039(31) | 205.850(33) | 0.031 ± 0.005 | ($M2 \leq 0.2\%$) |
| | $L_2$ | 182.921(31) | 205.876(33) | 0.015 ± 0.005 | $L_1/L_2, K/L_1$ |
| | Other | | | 0.023 | |
| | $\gamma$ | | 205.87(40) | 2.7 ± 0.15 | |
| | | | | 3.0 ± 0.2 | |
| 265.922(12) | $K$ | 140.940(6) | 265.925(14) | 1.74 ± 0.18 | $E1$ |
| (471.8 → 205.9) | $L_1$ | 242.103(6) | 265.914(14) | 0.35 ± 0.03 | anomalous |
| | $L_2$ | 242.970(9) | 265.925(15) | 0.15 ± 0.03 | conversion |
| | $L_3$ | | | ≤0.02 | |
| | $M_1$ | 259.790(17) | 265.926(21) | 0.12 ± 0.02 | |
| | $M_2$ | 260.180(68) | 265.927(68) | 0.023 ± 0.014 | |
| | Other | | | 0.048 | |
| | $\gamma$ | | 265.95(80) | 0.40 ± 0.04 | |
| | | | | 2.8 ± 0.2 | |
| 298.57(50) | $K$ | 173.589(45) | 298.574(46) | 0.024 ± 0.013 | $E1$ [g] |
| (504.4 → 205.9) | Other | | | 0.032 | anomalous |
| | $\gamma$ | | 298.5(300) | 0.080 ± 0.02 | conversion? |
| | | | | 0.14 ± 0.03 | |

TABLE II *(Continued)*

| Transition energy [keV(±eV)] [a] (initial → final state) | Shell [c] | Electron energy [keV(±eV)] [d] | Transition energy [keV(±eV)] [e] | Intensity [b] (% per $^{241}$Cm EC) | Multipolarity: mixing derived from: |
|---|---|---|---|---|---|
| 410.8(100) | $e^-$ | | | 0.008 | $E2$ scheme |
| (504.4 → 93.6) | $\gamma$ | | 410.8(100) | 0.087 ± 0.009 | |
| | | | | 0.095 ± 0.01 | |
| 417.24(40) | $K$ | 292.250(35) | 417.235(39) | 0.040 ± 0.016 | $E2 > 90\%$ |
| (623.1 → 205.9) | Other | | | 0.029 | $\alpha_K$ |
| | $\gamma$ | | 417.3(100) | 0.66 ± 0.04 | |
| | | | | 0.73 ± 0.04 | |
| 430.634(20) | $K$ | 305.641(7) | 430.626(20) | 0.208 ± 0.013 | $E2 > 97\%$ |
| (471.8 → 41.18) | $L_1$ | 406.858(37) | 430.669(41) | 0.034 ± 0.008 | $\alpha_K, \alpha_{L_1}$ |
| | Other | | | 0.14 | |
| | $\gamma$ | | 430.7(100) | 4.1 ± 0.2 | |
| | | | | 4.5 ± 0.2 | |
| 430(1000) | $e^-$ | | | ... | $E1$ scheme |
| (636.8 → 205.9) | $\gamma$ | | 430(1000) | ~0.04 | |
| | | | | ~0.04 | |
| 447.35(40) | $K$ | 322.366(36) | 447.351(40) | 0.04 ± 0.01 | $M1+E2$ (<40%) |
| (653.2 → 205.8) | Other | | | 0.01 | |
| | $\gamma$ | | 447.3(200) | 0.12 ± 0.015 | $\alpha_K$ |
| | | | | 0.17 ± 0.016 | |
| 463.273(20) | $K$ | 338.290(8) | 463.275(22) | 0.242 ± 0.018 | "(50 ± 6)% $E2$ |
| (504.4 → 41.18) | $L_1$ | 439.457(39) | 463.268(44) | 0.035 ± 0.008 | +50% $M1$" [g] |
| | Other | | | 0.034 | $\alpha_K, \alpha_{L_1}$ |
| | $\gamma$ | | 463.3(100) | 1.24 ± 0.08 | anomalous |
| | | | | 1.55 ± 0.08 | conversion? |
| 464.36(80) | $K$ | 339.38(70) | 464.36(80) | 0.011 ± 0.005 | $M1+E2$ |
| (670.2 → 205.9) | Other | | | ≤0.01 | $\alpha_K$ |
| | $\gamma$ | | 464.4(300) | 0.086 ± 0.01 | |
| | | | | 0.11 ± 0.02 | |
| 471.805(20) | $K$ | 346.820(2) | 471.805(21) | 13.1 ± 0.4 | $M1+E2$ |
| (471.8 → 0) | $L_1$ | 447.991(2) | 471.802(20) | 1.91 ± 0.09 | anomalous |
| | $L_2$ | 448.850(4) | 471.805(21) | 0.38 ± 0.02 | conversion |
| | $L_3$ | | | ≤0.08 | |
| | $M_1$ | 465.670(19) | 471.806(27) | 0.46 ± 0.03 | |
| | $M_2$ | 466.070(39) | 471.817(44) | 0.14 ± 0.03 | |
| | $N_1$ | 470.176(19) | 471.799(27) | 0.135 ± 0.012 | |
| | $N_2$ | | | 0.026 ± 0.012 | |
| | $N_3$ | | | ≤0.005 | |
| | $O_1$ | 471.472(58) | 471.845(62) | 0.052 ± 0.015 | |
| | Other | | | 0.036 | |
| | $\gamma$ | | 471.8(100) | 72 ± 3 | |
| | | | | 88 ± 3 | |
| 504.450(28) | $K$ | 379.465(18) | 504.450(28) | 0.058 ± 0.008 | "(72 ± 6)% $E2$ [g] |
| (504.4 → 0) | Other | | | 0.021 | +28% $M1$" |
| | $\gamma$ | | 504.4(100) | 0.60 ± 0.04 | $\alpha_K$ |
| | | | | 0.68 ± 0.04 | anomalous |
| | | | | | conversion? |
| 595.8(300) | $e^-$ | | | ... | $E2$ scheme |
| (636.8 → 41.2) | $\gamma$ | | 595.8(300) | 0.015 ± 0.003 | |
| | | | | 0.015 ± 0.003 | |
| 623.1(300) | $e^-$ | | | 0.005 | $M2$ scheme |
| (623.1 → 0) | $\gamma$ | | 623.1(300) | 0.012 ± 0.003 | |
| | | | | 0.017 ± 0.004 | |

TABLE II *(Continued)*

| Transition energy [keV(±eV)] [a] (initial → final state) | Shell [c] | Electron energy [keV(±eV)] [d] | Transition energy [keV(±eV)] [e] | Intensity [b] (% per $^{241}$Cm EC) | Multipolarity: mixing derived from: |
|---|---|---|---|---|---|
| 636.88(25) | $K$ | 511.896(11) | 636.881(27) | 0.176 ± 0.018 | (24 ± 12)% $E2$ |
| (636.9 → 0) | $L_1$ | 613.059(61) | 636.870(62) | 0.030 ± 0.008 | +76% $M1$ |
| | Other | | | 0.017 | $\alpha_K$ |
| | $\gamma$ | | 636.8(100) | 1.55 ± 0.11 | |
| | | | | 1.77 ± 0.11 | |
| 652.1(400) | $e^-$ | | | 0.003 | $M1$ scheme |
| (652.1 → 0) | $\gamma$ | | 652.1(400) | 0.04 ± 0.01 | |
| | | | | 0.043 ± 0.01 | |
| 653.2(200) | $e^-$ | | | 0.001 | $E1$ scheme |
| (653.2 → 0) | $\gamma$ | | 653.2(200) | 0.15 ± 0.01 | |
| | | | | 0.15 ± 0.01 | |
| 670.2(200) | $e^-$ | | | 0.006 | $E1$ scheme |
| (670.2 → 0) | $\gamma$ | | 670.2(200) | 0.58 ± 0.04 | |
| | | | | 0.59 ± 0.04 | |

[a] Weighted averages of column 4. Errors (standard deviations) take into account correlated contribution from calibration uncertainty.

[b] Errors include line-area-statistical and decay correction uncertainties, but do not include electron detector efficiency uncertainties, so that subshell-ratio uncertainties can be obtained from this column.

[c] Notation "other" or "$e^-$" indicates intensities are calculated from theoretical internal conversion coefficients for shells not listed and for those where only upper limits are indicated.

[d] Errors are those from line position only.

[e] Errors include line position, binding energy, and calibration constant uncertainties.

[f] Intensity calculated from theoretical conversion coefficient.

[g] Multipolarity admixture moot, probable anomalous conversion; cf. Sec. IV C.

tector, a bare cleaved-surface NaI(Tl) crystal mounted directly on a photomultiplier, was determined from pulse-height analysis[11] at various energies between 5 and 120 keV. In the 5–20 keV energy range the efficiency varies from 50 to 80% and is known to an accuracy of ~10%. Table II summarizes all $\gamma$, $e^-$, and transition energies, intensities, and multipolarities.

In order to maintain continuity of discussion of information relevant to the nuclear decay scheme, we present other electron-spectroscopic results [near-threshold $M1$ $K$-shell internal conversion coefficients (ICC), $P_1$ subshell theoretical ICC, and nuclear penetration contributions to anomalous $M1$ and $E1$ internal conversions] in Sec. IV C, and on $K$-Auger spectra and $K$-shell fluorescent yield in Sec. V. Selected examples of conversion lines are illustrated in Figs. 7, 10, and 11 in these sections.

### C. Coincidence measurements

A two-parameter $\gamma$-$\gamma$ coincidence experiment was performed with 4- and 17-cm$^3$ Ge(Li) diodes. The resolving time ($2\tau$) of the coincidence circuit was 300 nsec. Single-channel analyzers on both parameters were set to exclude the Am $K\alpha$ and $K\beta_1'$ x-ray peaks from the gates in order to reduce the chance coincidence rate. Coincidence events recorded on a magnetic tape were later read back into the analyzer memory through a digital gate system, with which any desired $\gamma$-ray gate could be selected. All statistically significant $\gamma$-ray spectra obtained in coincidence with each of the $\gamma$ rays listed in Table I as gates are given in Table III. The $\gamma$-ray spectrum measured with the 17-cm$^3$ Ge(Li) detector and gated by the 205.9 keV photopeak is shown in Fig. 4. The energies of the 298.5, 430, and 464.4 keV $\gamma$ rays were determined from this spectrum, using the 266.0, 417.3, and 471.8 keV $\gamma$ rays as standards. The presence of the 417.3, 447.3, and 464.4 keV transitions in the coincidence spectrum confirms the existence of levels at 623.1, 653.2, and 670.2 keV in $^{241}$Am, since the 205.9 keV level is established via $^{245}$Bk $\alpha$ decay.

The weak 164.8 keV transition could not be resolved from the strong 165.0 keV transition in the $\gamma$ spectra or seen in the conversion electron singles spectra. The intensities of the 151.4 and 165.0 keV $\gamma$ rays were determined from a spectrum gated by the 471.8 keV photopeak, which is not in

TABLE III. Results of two-parameter $\gamma$-$\gamma$ coincidence experiment.

| $\gamma$-ray gate [a] (keV) | $\gamma$ rays [b] (keV) |
|---|---|
| 132.4 | 205.9, 430.7, 463.3, 471.8, 504.4, and Am $K$ x rays |
| 164.8+165.0 | 205.9, 266.0, 417.3, 430.7, 447.3, 471.8, and Am $K$ x rays |
| 205.9 | 266.0, 298.5, 417.3, 430, 447.3, 464.4, and Am $K$ x rays |
| 417.3 | 164.8, 205.9, and Am $K$ x rays |
| 430.7 | 132.4, 165.0, 180.3, and Am $K$ x rays |
| 471.8 | 132.4, 151.4, 165.0, 180.3, and Am $K$ x rays |
| 504.4 | 132.4 and Am $K$ x rays |

[a] Each gate included only the symmetric part of the photopeak.

[b] The $\gamma$-ray energies are those measured from $\gamma$-singles spectra.

cascade with the 164.8 keV transition. These intensities were measured relative to that of the 132.4 keV $\gamma$ ray which was taken as 3.9% per $^{241}$Cm EC decay. The energy and intensity of the 164.8 keV $\gamma$ ray was obtained from a spectrum gated by the 417.3 keV photopeak, its intensity being measured with respect to that of the 205.9 keV $\gamma$ ray, after subtracting the chance coincidence contribution of the 165.0 keV peak from its area. The relative intensities of the 164.8 and 205.9 keV $\gamma$ rays thus determined are in agreement with the values obtained by Ahmad[3] from $^{245}$Bk $\alpha$ decay, which feeds the 164.8 keV but not the 165.0 keV transition.

A $\gamma$-ray spectrum was also measured in coincidence with the Am $K\alpha$ peak. This spectrum was found to contain all the prominent $\gamma$ rays listed in Table I except the $\gamma$ rays connecting the 652.1, 653.2, and 670.2 keV levels to the ground state. This indicates that these levels are populated by $L, M, \ldots$ but not by $K$ electron capture. Also by comparing the relative intensities of 636.8 and 471.8 keV $\gamma$ rays in the coincidence and singles spectra it was found that only $3 \pm 1\%$ of the feed to the 636.8 keV level occurs by $K$ electron capture. These observations are consistent with the calculated $Q_{EC} = 0.77$ MeV and the $K$ binding energy of ~125 keV.

### D. $\alpha$ spectroscopy of $^{245}$Bk

Several $\alpha$-particle spectra of a $^{245}$Bk sample were measured with a 6-mm-diam Au-Si surface-barrier detector. A typical spectrum taken at a source-to-detector geometry of ~2% is shown in Fig. 5. The $\alpha$-particle energies were measured with respect to $^{244}$Cm (5.805 MeV) and $^{242}$Cm (6.111 MeV) standards.[12] The $\alpha$-particle energies and intensities obtained from these measurements

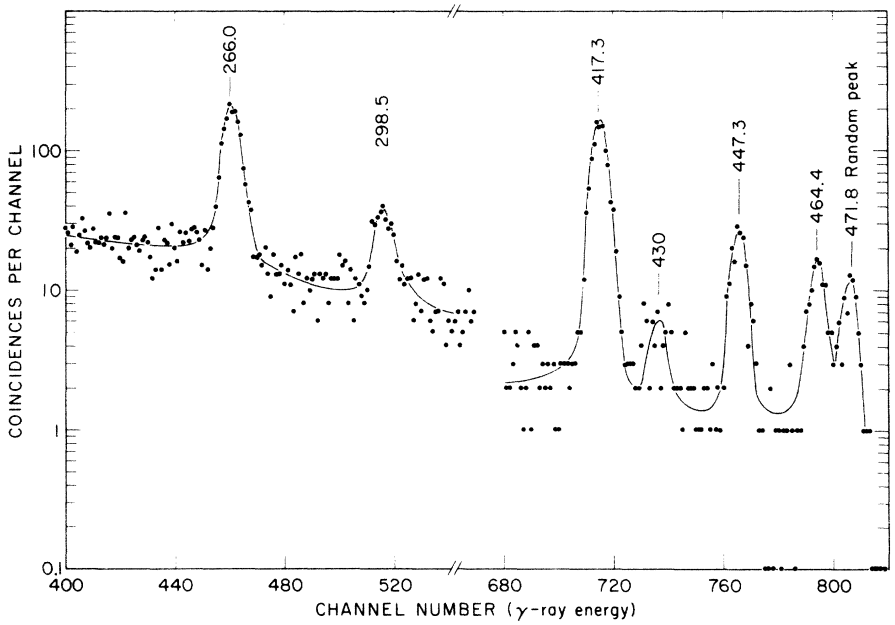


FIG. 4. $^{241}$Cm $\gamma$-ray spectrum measured with a 17-cm$^3$ Ge(Li) detector in coincidence ($2\tau = 300$ nsec) with the 206-keV photopeak. The spectrum for gate selection was measured with a 4-cm$^3$ Ge(Li) diode. The $\gamma$-ray energies shown in the figure are those determined from the $\gamma$-singles spectrum. Zero events are plotted at 0.1. Random coincidences (only those with 472 keV transition are visible) have not been subtracted.

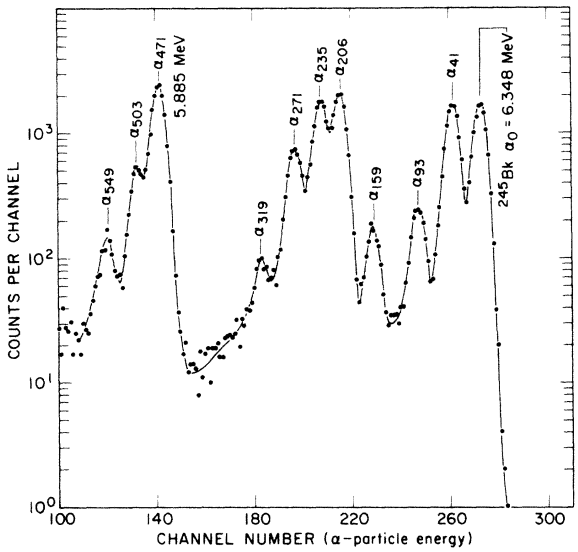


FIG. 5. $^{245}$Bk $\alpha$ spectrum measured with a 6-mm-diam Au-Si surface-barrier detector at a source-to-detector geometry of ~2%. The energy and intensity of the $\alpha_{375}$ group was determined from another spectrum counted longer.

are given in Table IV, and are in good agreement with the values reported by Ahmad.[3] The hindrance factors were calculated from Preston's equations[13] using a half-life of 5.0 days, an $\alpha$ branching of 0.1%, and a radius parameter of 9.100 fm.

### E. Half-life and $\alpha$ branching

The half-life of $^{241}$Cm was measured by following the decay of the 471.8 keV $\gamma$ ray on a Ge(Li) spectrometer for a period of 66 days. A least-squares fit analysis to plotted-peak areas gave a half-life of 32.8 ± 0.2 days.

We observed the $L_2$ and $L_3$ conversion lines of the 145.536 ± 0.009 keV transition in $^{237}$Pu following the weak $\alpha$-decay branch of $^{241}$Cm. This isomeric $E3$ ($\frac{1}{2}+ \rightarrow \frac{7}{2}-$) transition with $T_{1/2} = 0.18$ sec exhibited no Doppler distortion of the line shapes. Doppler shift of the conversion electron emitted from the moving recoil in that half of the decays in which the recoil is ejected into the spectrometer vacuum (and is thus not stopped) produces a shoulder on the line extending several linewidths to higher energy. However in this case the recoils have moved out of the source region of the spectrometer before the delayed emission occurs, so this distorting half of the line intensity is not seen. We therefore double the observed intensity and obtain the total transition intensity by including conversion-electron intensity from shells not observed as given by theoretical $E3$ values.

Since all the excited states decay through the 145.5 keV transition its intensity is the same as the total $\alpha$ population to these states. After making a correction for the $\alpha$ intensities to the ground state band[14] of $^{237}$Pu, the $\alpha/(\alpha + EC)$ ratio was found to be 0.010 ± 0.001. This is in good agreement with the previously reported value[15] of 0.0096 ± 0.0009.

TABLE IV. $^{245}$Bk $\alpha$ groups.

| Energy (MeV) | Excited state energy (keV) | Intensity (%) | Hindrance factor |
|---|---|---|---|
| 6.348 ± 0.004 | 0 | 15.5 ± 0.5 | $6.3\times10^2$ |
| 6.308 ± 0.004 | 41 | 15.0 ± 0.5 | $4.2\times10^2$ |
| 6.257 ± 0.004 | 93 | 1.5 ± 0.1 | $2.4\times10^3$ |
| 6.192 ± 0.004 | 159 | 1.2 ± 0.1 | $1.4\times10^3$ |
| 6.145 ± 0.004 | 206 | 18.3 ± 0.5 | 55 |
| 6.117 ± 0.004 | 235 | 15.2 ± 0.5 | 48 |
| 6.081 ± 0.004 | 271 | 6.2 ± 0.3 | 77 |
| 6.034 ± 0.004 | 319 | 0.55 ± 0.08 | $5.0\times10^2$ |
| 5.979 ± 0.005 | 375 | 0.08 ± 0.02 | $1.8\times10^3$ |
| 5.885 ± 0.004 | 471 | 21.5 ± 0.5 | 2.1 |
| 5.853 ± 0.004 | 503 | 4.1 ± 0.2 | 7.5 |
| 5.808 ± 0.004 | 549 | 0.9 ± 0.1 | 19 |

## IV. DISCUSSION

### A. Decay scheme

The electron capture decay scheme of $^{241}$Cm and $\alpha$-decay scheme of $^{245}$Bk deduced from the present investigation are shown in Fig. 6. For the $^{241}$Cm EC decay, all energy balances up to the 652 keV level for stopover sums versus crossover transitions lie within a maximum disparity of 6 eV except for two cases which agree within 30 eV, less than one standard error. These balances, combined with the coincidence data for energies above the Am $K$ x rays unambiguously imply the indicated levels and transition ordering.

#### 1. *Ground-state* $\frac{5}{2}-[523]$ *band*

The ground-state spin of $^{241}$Am has been measured to be $\frac{5}{2}$ by the atomic beam method.[16] From its $\alpha$ decay to $^{237}$Np it is reasonably certain that it is the $\frac{5}{2}-[523]$ Nilsson state. Four members of the $^{241}$Am ground-state band have been identified via their population in the $^{245}$Bk $\alpha$ decay. The observed energies of the rotational members fit well with the values calculated by the Bohr-Mottelson[17] formula. The absence of an observable outfeed from the 93.4 keV level to match the 0.09% infeed by the 410.8 keV transition in the $^{241}$Cm decay is consistent with the small conversion-electron and $\gamma$-ray intensities predicted for the 93.4 and 52.2 keV depopulating transitions. Electron

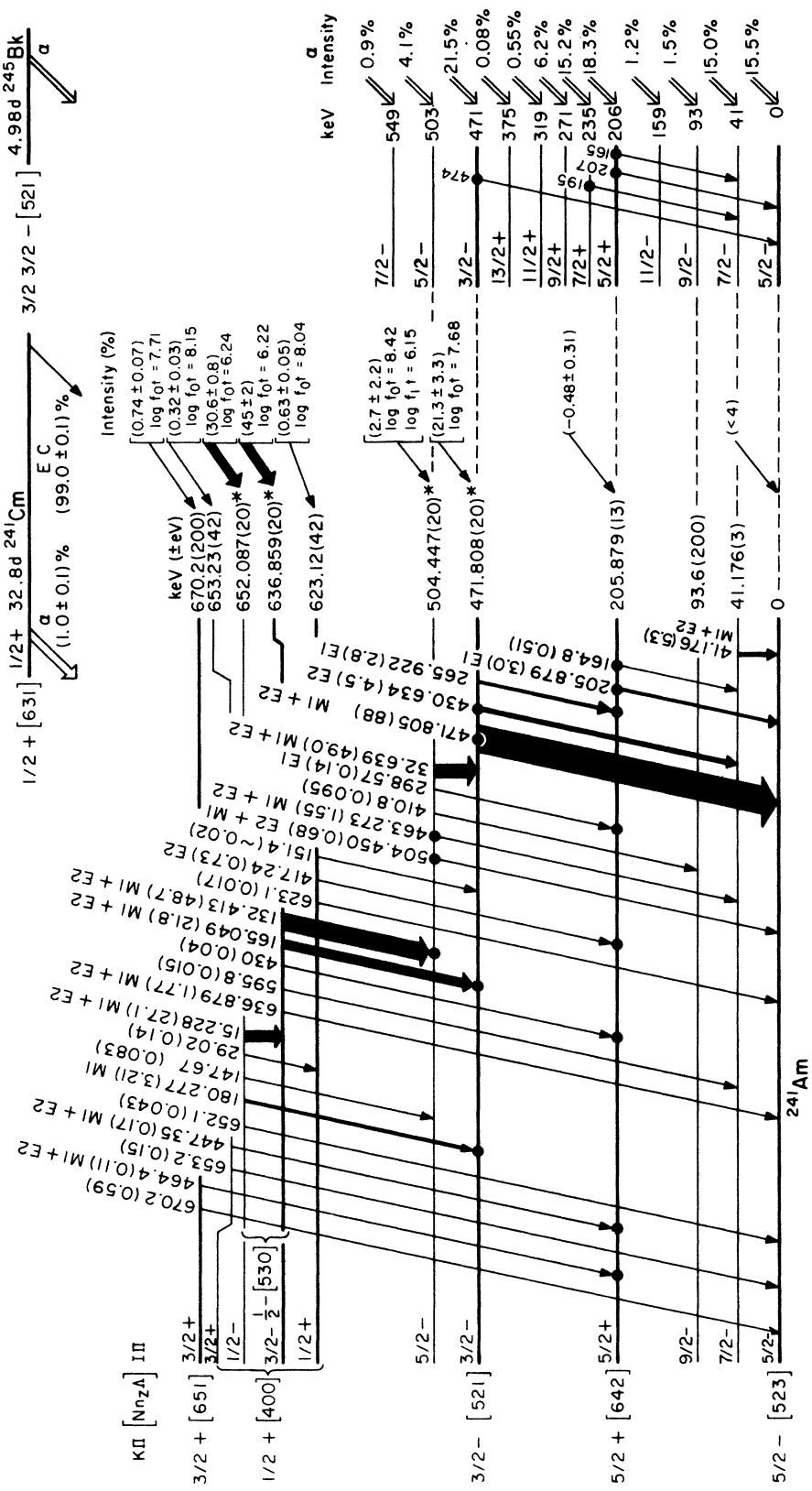


FIG. 6. Level scheme of $^{241}$Am populated by electron capture in $^{241}$Cm and $\alpha$ decay of $^{245}$Bk. Transition intensities in percent per EC decay of $^{241}$Cm are in parentheses following transition energy in keV. Energies of four levels marked with asterisk (*) were determined via a weighted least-squares fitting program involving accurate difference transitions in 20 independent expressions. Other level energies are weighted averages. A large part of the error in each level energy is a correlated electron spectrometer calibration constant contribution, increasing from 3 eV at the 206 keV $K$ line to 15 eV at the 470 keV $K$ line and 20 eV at the 636 keV $K$ line. Intraband transitions are shown by vertical arrows; interband by slanted arrows. At the right are shown the levels populated with the indicated intensities by $\alpha$ decay of $^{245}$Bk; the level energies at the right are from the $\alpha$ spectroscopy, and the spins of levels not seen via $^{241}$Cm decay are inferred from the $\alpha$ hindrance factors of Table VI. Four $\gamma$ transitions seen (Ref. 3) in coincidence with $\alpha$ particles are shown on these $\alpha$-fed levels. $\gamma$-$\gamma$ coincidences shown by dots.

capture decay to this and higher rotational levels is third forbidden, thus unobservably weak.

### 2. $\frac{3}{2}-[521]$ band

The level at 471.8 keV decays to the ground state by an $M1$-$E2$ transition and to the $\frac{7}{2}-$ member of the ground-state band by a >97% $E2$ transition. Hence a reasonable spin-parity assignment for the 471.8 keV state is $\frac{3}{2}-$. This state is also populated by the favored $\alpha$ group of $^{245}$Bk (hindrance factor = 2.1) and hence it should have the same single-particle configuration as the $^{245}_{97}$Bk ground state. From the Nilsson diagram[2] the ground state for the 97th proton is expected to be the $\frac{3}{2}-[521]$ or $\frac{7}{2}+[633]$ orbital. Hence the $^{245}$Bk ground state and the 471.8 keV state of $^{241}$Am are given Nilsson-state assignments of $\frac{3}{2}-[521]$. The level at 504.4 keV decays by $M1$-$E2$ transitions to the $\frac{5}{2}-$ and $\frac{7}{2}-$ members of the ground-state band and by an $M1$ transition to the 471.8 keV level. Hence its spin-parity must be $\frac{5}{2}-$; it has been assigned as the $\frac{5}{2}-$ member of the $\frac{3}{2}-[521]$ rotational band. This assignment is supported by the low hindrance factor of the $\alpha$ transition populating it; similarly the 549 keV state is assigned as the $\frac{7}{2}-$ rotational member (cf. Table IV). The latter state is not expected to be populated via EC (third forbidden) or by decay of the higher levels fed via EC decay.

### 3. $\frac{5}{2}+[642]$ band

In a $\gamma$-ray spectrum gated by 6.00 to 6.18 MeV $^{245}$Bk $\alpha$ particles (feeding levels from 206 to 375 keV excitation) Ahmad[3] observed Am $K$ x rays and 207.4, 195, and 165.5 keV $\gamma$ rays. The high intensity of the 165.5 keV $\gamma$ ray (7% per $\alpha$ decay) clearly indicates that it is the 207.4 → 41.2 transition. (In the present work its energy is identified as 164.8 keV.) The observed low $K$ x-ray intensity in the $\alpha$-$\gamma$ coincidence measurement is consistent only with $E1$ or $E2$ multipolarity for the two transitions. Since the multipolarity of the 205.9 keV transition has been established as $E1$ in the present experiments, the multipolarity of the "165.5" keV transition must also be $E1$. Hence the spin-parity of the 205.9 keV level can only be $\frac{5}{2}+$ or $\frac{7}{2}+$. The observation of an anomalous 265.9 keV $E1$ transition (see Sec. IV C) from the 471.8 keV level to this state makes it a $\frac{5}{2}+$ state. This is consistent also with the absence of observed transition to the 93.6 keV, $\frac{9}{2}-$ level. The 205.9 keV level has been given a Nilsson-state assignment of $\frac{5}{2}+[642]$ because this state is expected to lie in this energy region; it is identified in $^{243}$Am (Ref. 6) and $^{245}$Am (Ref. 3). Five members of this rotational band have been identified in the $^{245}$Bk $\alpha$ decay (Fig. 5), and the 195 keV (236 keV → 41 keV) transition was seen in $\alpha$-$\gamma$ coincidence. The observed energies of these levels indicate that the level spacings have been highly compressed (rotational constant = 4.2 compared to the normal value of ~6.0). This contraction in the band structure is accounted for in terms of the strong Coriolis interaction[18] between the $\frac{5}{2}+[642]$ and $\frac{7}{2}+[633]$ single-particle states; the latter band head has been estimated to be at 590 keV based on observed $I = \frac{9}{2}, \frac{11}{2}$, and $\frac{13}{2}$ members of the band in nuclear reaction studies.[19] Similar distortions in the $\frac{5}{2}+[642]$ band have also been observed in $^{243}$Am (Ref. 6) and $^{245}$Am (Ref. 3) and these have been quantitatively explained in terms of Coriolis mixing.

The 195 keV transition seen[3] in coincidence with selected $\alpha$ particles is assigned as the 235 keV → 41 keV transition. Its low intensity, ~1% per decay compared to ~15% $\alpha$ feed to the 235 keV level, then requires that the unobserved 29 keV $M1$ transition to the 206 keV level carries ~14 times as much intensity as the 195 keV $E1$ transition. An $E1$ retardation relative to single particle rates of ~2000 would yield the observed 195 keV intensity. Such an $E1$ retardation factor is modest for heavy element $E1$ transitions, and small compared to observed $E1$ retardations associated with anomalous internal conversion.[20] Since similar retardation factors are expected for the 206 keV (and 165 keV) $E1$ transitions, normal $E1$ conversion is predicted and observed (see Sec. IV C).

### 4. $\frac{1}{2}-[530]$ band

The multipolarities of the 180.3 ($M1$) and 147.7 ($E2$) keV transitions make the 652.1 keV level a $\frac{1}{2}-$ state. The 636.8 keV level decays to the $\frac{3}{2}-$ and $\frac{5}{2}-$ members of the $\frac{3}{2}-[521]$ band by $M1$ transitions. Hence this state should have spin-parity of $\frac{3}{2}-$ or $\frac{5}{2}-$. The existence of a 15.2 (652.1 → 636.8) keV $M1$ transition makes this level a $\frac{3}{2}-$ state. The $\frac{3}{2}-$ assignment is consistent with the measured $M1+E2$ multipolarity of the 636.8 keV $\gamma$ ray. We interpret the 636.8 keV level as the $\frac{3}{2}-$ member of the $\frac{1}{2}-$ rotational band with band head at 652.1 keV. The level spacing between the $\frac{1}{2}-$ and $\frac{3}{2}-$ states fixes the sign of the decoupling parameter $a$ as negative and its numerical value as greater than 1. Assuming a typical rotational constant of 6.0 keV for this band one obtains the value of $a$ as −1.8. The theoretical values of $a$ for the possible $\frac{1}{2}-$ Nilsson states are: $\frac{1}{2}-[530]$, −2.4; $\frac{1}{2}-[770]$, −7.7; $\frac{1}{2}-[521]$, +1.1. On this basis we choose a $\frac{1}{2}-[530]$ assignment for the 652.1 keV state. A $K\pi = \frac{1}{2}-$ band has also been observed in

$^{237}$Np (Ref. 21) at 281.4 keV and it has been assigned to the same Nilsson state.

### 5. $\frac{1}{2}$+[400] band

The $E2$ multipolarity of the 417.2 keV transition and the absence of any other transition to the members of the $\frac{5}{2}$+[642] rotational band indicate that the 623.1 keV level has a spin-parity of $\frac{1}{2}$+. The $M1$ multipolarity of the 447.3 (653.2 − 205.9) keV transition restricts the spin-parity of the 653.2 keV level to $\frac{3}{2}$+, $\frac{5}{2}$+, or $\frac{7}{2}$+. The fact that this state receives direct EC population makes it a $\frac{3}{2}$+ state. This spin assignment is consistent with the absence of any other transition from this state to the members of the $\frac{5}{2}$+[642] band. We interpret this state as the $\frac{3}{2}$+ member of the $\frac{1}{2}$+ rotational band based at 623.1 keV. The level spacing between these two states fixes the sign of the decoupling parameter $a$ as positive for any reasonable choice of rotational constant. A value of 6.0 keV for the rotational constant gives the value of $a$ as +0.7. The theoretical values of $a$ for possible $\frac{1}{2}$+ Nilsson states are: $\frac{1}{2}$+[400], +0.6; $\frac{1}{2}$+[651], −1.0; $\frac{1}{2}$+[660], +6.6. On this basis we assign the 623.1 keV level to the $\frac{1}{2}$+[400] Nilsson state. This state has also been identified in $^{237}$Np at 332.4 keV.[21]

### 6. $\frac{3}{2}$+[651] band

Since the 670.2 keV level receives direct EC feed its spin can only be $\frac{1}{2}$ or $\frac{3}{2}$. The $M1$ multipolarity of the 464.4 keV transition establishes the spin-parity assignment as $\frac{3}{2}$+, which is consistent with an observable $E1$ transition rate for the 670.2 keV transition. The $\frac{3}{2}$+ single-particle states in the vicinity are the $\frac{3}{2}$+[651] and the $\frac{3}{2}$+[402] hole states, which intersect very near the region of deformation ($\epsilon \sim 0.27$) expected here. Allowed electron capture to both of these states violates the Alaga[22] asymptotic quantum number selection rules; for the $\frac{3}{2}$+[651] state by two units in $\Delta n_z$, and for the $\frac{3}{2}$+[402] state by one unit in $\Delta\Lambda$, by three in $\Delta n_z$, and by two units in $\Delta N$. As $\log f_0 t = 7.71$ characterizes a hindrance of 10–100 for the allowed electron capture corresponding reasonably to the two unit (rather than six) selection rule violation of the $\frac{3}{2}$+[651] state, this is the assignment chosen.

### 7. *Proton transfer studies*

The energy levels of $^{241}$Am have recently been investigated by proton transfer reactions by Erskine *et al.*[19] Their results are consistent with our proposed decay scheme. The $\frac{7}{2}$+[633] band they observe (band head estimated to be at 590 keV) would, in our experiments, be expected to receive very little direct feed via the first forbidden unique EC transition or indirectly via fairly low energy interband $E2$ transitions from the weakly populated high lying $\frac{3}{2}$+ states. Their calculations yield low probability for population by proton transfer to the $\frac{1}{2}$−[530] and $\frac{3}{2}$+[651] hole states, which they do not observe.

## B. Electron capture transition probabilities

The EC population to a $^{241}$Am level was determined from the difference between the $\gamma$-ray plus conversion-electron outfeed and infeed at that level. The intensity in percent per EC decay was obtained by normalizing the total $\gamma$ and conversion-electron intensities to the ground state as 100%. The intensities are given in Fig. 6. Log$f_0t$ values ($f_0$ for allowed and forbidden but not unique transitions) were calculated[23] with a value for the available EC decay energy[24] of 772 keV between ground states. Contributions from shells other than $K$ and $L_1$ were taken into account[25] as was the neutrino energy dependence of the capture probabity ratios for the several shells. For the first forbidden unique transitions $f_1t$ was determined from $f_1t = (q_K^2/12) f_0t$, $q_K$ the neutrino energy in $K$-shell EC, and both the $L_1$ and $L_3$ EC contributions were evaluated appropriately for first forbidden unique transitions.

The number of $K$-shell holes created by internal conversion and electron capture to the excited states is calculated to be (81 ± 3)% per EC decay. The observed $K$ x-ray and $K$-Auger-electron intensities yield the number of $K$ holes as (82 ± 5)% per EC decay. This agreement indicates ≤6% EC feed to the $^{241}$Am ground state. EC to the ground state is a first forbidden unique transition with an expectation value for $\log f_1t \sim 8.5$, which corresponds to a ~4% EC branching ratio, in agreement with our measured limit. Even less EC may be expected, as the transition violates the Alaga[22] selection rules for a first forbidden unique decay by two units in $N$ and $n_z$. The EC feed to the 205.9 keV level is found to be (−0.4 ± 0.3)%, consistent with the expectation of a very small EC branch for this second forbidden transition. Here again the Alaga[22] rules are violated by one unit in $n_z$. Both these EC branches are ignored in our evaluation.

The theoretical[25] ($K$/total) capture ratio for the 636.8 keV state is 0.03, in excellent agreement with our measured value (cf. Sec. III C) of 0.03 ± 0.01. No observable EC is expected to the $\frac{5}{2}$ or higher spin members of the $\frac{1}{2}$+ or $\frac{1}{2}$− band.

If the spin assignments are correct, the EC to the 504.4 keV level is first forbidden unique. On this basis the measured EC feed of (2.7 ± 2.2)% corresponds to a $\log f_1t$ value of $6.15 \pm ^{0.75}_{0.25}$. The

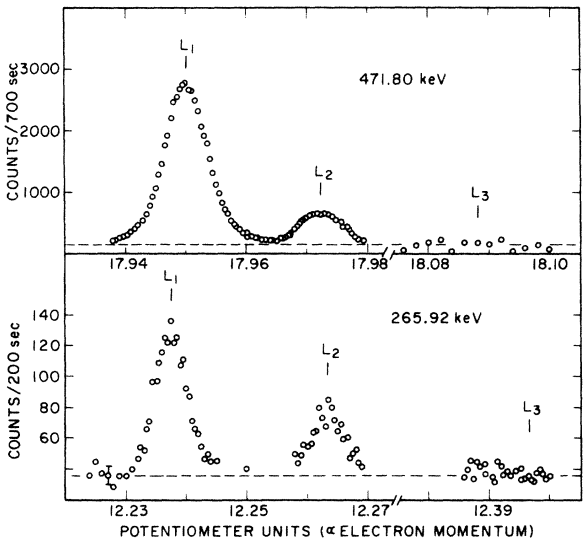


FIG. 7. The $L$-subshell conversion lines from the 471.80 ($M1+E2$) and the 265.92 keV ($E1$) transitions. The vertical marks with subshell labels are the calculated line peak positions. Both these transitions exhibit anomalous conversion intensity. The $L_2$ 471.8 absolute conversion coefficient is ~40% smaller than the theoretical $M1$ value. The $L_1$ and $L_2$ 265.9 conversion coefficients are ~150 and 200 times larger than the theoretical $E1$ values.

upper $\sigma$ limit of 6.90 is low for a first forbidden unique transition, but a small increase in the intensity error could raise the $\log f_1 t$ value to the expected range of ~8.5.

It is noteworthy that the two bands receiving the preponderance of EC, the $\frac{1}{2}-[530]$ to which the first forbidden EC totals 75%, and the $\frac{3}{2}-[521]$ which gets 22% of first forbidden EC, are the only bands in $^{241}$Am that satisfy the Alaga[22] deformed nucleus asymptotic quantum number selection rules. In this respect the high $\log f_0 t$ for the capture to the 471.8 keV, $\frac{3}{2}-[521]$ band head is anomalous, suggesting a mixed band character. As noted, allowed capture (by $I\pi$ rules) to the $\frac{1}{2}+[400]$ and $\frac{3}{2}+[651]$ bands violates the Alaga rules; the former in extreme fashion, by six units; its $f_0 t$ value is raised by two orders of magnitude compared to the first forbidden decay to the $\frac{1}{2}-[530]$ band.

### C. Internal conversion anomalies and γ-ray transition probabilities

#### 1. *266 keV E1 anomaly*

It is clear from the internal conversion coefficients (ICC) and the shell ratios in Table V that the 265.9 keV transition is not a normal $E1$ transition (cf. Fig. 7); the anomaly factors (experimental ICC/ordinary $E1$ ICC)[26] lying between 100 and 200 are the largest known. The results cannot be explained with $E1+M2$ mixing; the $L_2$ ICC is even larger than the $M2$ value, and the upper limit on $L_3$ ICC is inconsistent with the $\geq$70% $M2$ component required by $K$, $L_1$, and $M1$ ICC's. That it is $E1$ ($+M2$?) and not $M1+E2$ is established by the certain multipolarities of the 430 keV ($E2$) and 206 keV ($E1$) transitions, which fix the $\frac{3}{2}-[521]$ and $\frac{5}{2}+[642]$ band parities as opposite.

Anomalous conversion coefficients for $E1$ transitions are known[20] to occur in the heavy-element region. These transitions exhibit anomaly in $K$, $L_1$, $L_2$, $M_1$, and $M_2$ conversion coefficients but their $L_3$ and $M_3$ conversion coefficients are normal. Thus the $L_3$ and $M_3$ conversion coefficients can be used to deduce $M2$ admixtures in such transitions. In the present experiments we have measured only an upper limit on the $L_3$ conversion coefficient, from which an upper limit of 50% $M2$ admixture has been deduced.

Nilsson and Rasmussen[27] have developed selection rules for spheroidally deformed nuclei which

TABLE V. Internal conversion of the 265.9 keV transition in $^{241}$Am.

| Shell or ratio | Experimental ICC | Theoretical [a] ICC $E1$ | Theoretical [a] ICC $M2$ | $E1$ anomaly factor (col 2/col 3) |
|---|---|---|---|---|
| $K$ | 4.3 ±0.6 | 0.0437 | 4.47 | 98±14 |
| $L_1$ | 0.87±0.12 | 0.005 88 | 1.24 | 148±11 |
| $L_2$ | 0.38±0.08 | 0.001 95 | 0.193 | 195±40 |
| $L_3$ | ≤0.05 | 0.001 20 | 0.118 | |
| $M_1$ | 0.30±0.05 | 0.001 36 | 0.318 | 220±35 |
| $M_2$ | 0.06±0.04 | 0.000 491 | 0.0552 | 122±80 |
| $L_1/L_2$ | 2.3 ±0.4 | 3.02 | 6.42 | |
| $L_1/L_3$ | ≥17 | 4.90 | 10.5 | |
| $K/L_1$ | 4.9 ±0.7 | 7.43 | 3.60 | |
| $K/L_2$ | 11 ±2 | 22.4 | 23.2 | |

[a] R. S. Hager and E. C. Seltzer, Ref. 26.

TABLE VI. Internal conversion of the 471.8 keV transition in $^{241}$Am.

| Shell or ratio | ICC Experiment | Theory [a] $E2$ | Theory [a] $M1$ |
|---|---|---|---|
| $K$ | 0.181 ± 0.009 | 0.0360 | 0.321 |
| $L_1$ | 0.0265 ± 0.0018 | 0.007 19 | 0.0566 |
| $L_2$ | 0.005 27 ± 0.000 37 | 0.0113 | 0.007 52 |
| $M_1$ | 0.0064 ± 0.0005 | 0.001 79 | 0.0136 |
| $M_2$ | 0.0019 ± 0.0005 | 0.003 07 | 0.002 04 |
| $L_1/L_2$ | 5.02 ± 0.17 | 0.636 | 7.53 |
| $K/L_2$ | 34 ± 2 | 3.18 | 42.7 |
| $M_1/M_2$ | 3.3 ± 0.9 | 0.583 | 6.67 |

[a] R. S. Hager and E. C. Seltzer, Ref. 26.

predict which transitions may be expected to exhibit anomalous conversion. Their asymptotic quantum number selection rules applied to the 266 and 298 keV transitions between the $\frac{3}{2}-[521]$ and $\frac{5}{2}+[642]$ bands yield both the radiative transition retardation and the allowed penetration matrix elements necessary for significantly anomalous $E1$ conversion. Similarly for the mixed $M1$-$E2$ transitions of 472, 504, and 463 keV between the $\frac{3}{2}-[521]$ and the $\frac{5}{2}-[523]$ ground-state bands, the Nilsson-Rasmussen rules indicate photon retardation and allowed "penetration" conversion, hence anomalous conversion is expected, and observed. On the other hand the 206 and 164 keV $E1$ photon transitions from the $\frac{5}{2}+[642]$ to the $\frac{5}{2}-[523]$ bands are also retarded but penetration conversion is not allowed by these selection rules. As noted in Sec. IV A 3., these transitions are probably retarded by factors, relative to single-particle rates, that are typical of most $E1$ transitions, not associated with the asymptotic quantum number rules. The 206 keV transition exhibits normal $E1$ conversion.

Analyses of the cases of anomalous conversion can be made with the inclusion of penetration corrections developed by Church and Weneser.[28] Using the parametrization of Hager and Seltzer[29] the electric and magnetic ICC's can be written

$$\text{Electric ICC} = \alpha(E)(1 + A_1\lambda_1 + A_2\lambda_1^2 + A_3\lambda_2 + A_4\lambda_2^2 + A_5\lambda_1\lambda_2 + A_6\lambda_3 + A_7\lambda_1\lambda_3), \quad (1)$$

$$\text{Magnetic ICC} = \beta(M)(1 + B_1\lambda + B_2\lambda^2), \quad (2)$$

where $\alpha(E)$ and $\beta(M)$ are the normal (no penetration) ICC's, $A_i$ and $B_i$ are coefficients calculated (Hager and Seltzer[29]) from electron wave functions for the multipolarity of interest, and the $\lambda$ and $\lambda_i$ are the magnetic and electric penetration parameters, respectively. The penetration parameters

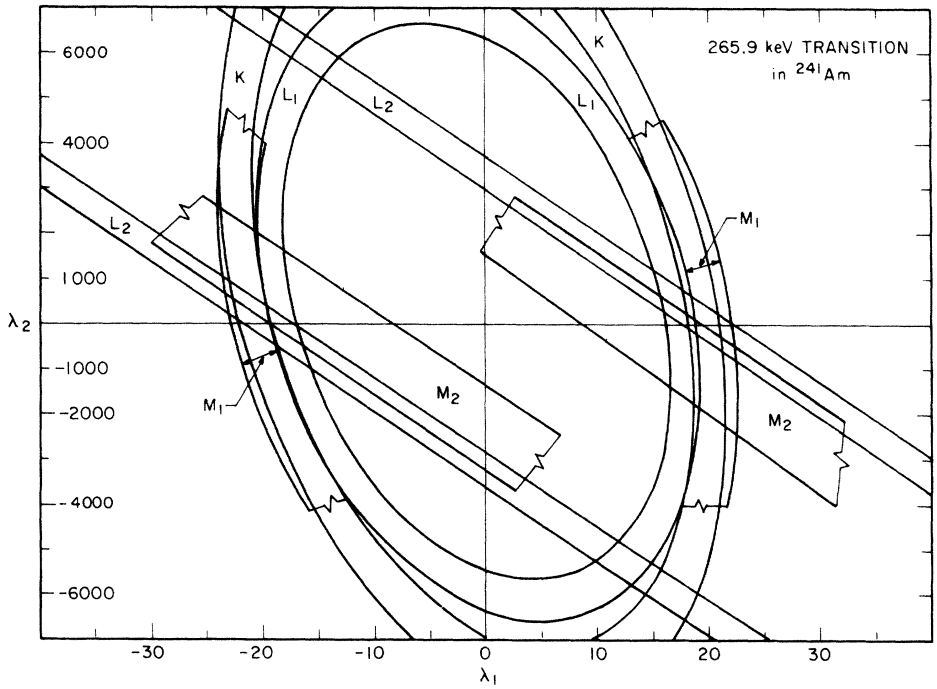


FIG. 8. $E1$ (no $M2$ mixing) penetration parameter analysis of the internal conversion of the 265.9 keV transitions in $^{241}$Am. Each subshell conversion coefficient with its experimental error generates a conic section [Eq. (1)] band in the $(\lambda_1, \lambda_2)$ plane, whose near intersections in the vicinity of (18.5, 283) and (−19.3, −63) yield satisfactory minimal weighted-least-squares residuals.

depend on nuclear structure and are to be determined from an analysis of the experimental quantities.

For the 265.9 keV transition we first assume the $M2$ mixing is negligible and use only $\lambda_1$ and $\lambda_2$ parameters in Eq. (1). Figure 8 shows that there are two regions of the $(\lambda_1, \lambda_2)$ plane where the conic sections overlap indicating consistency among the experimental values. Weighted $(1/\sigma^2)$ least-squares minimization using the experimental quantities of Table V yields the two regions

$$\lambda_1 = 18.5, \quad \lambda_1 = -19.3,$$

$$\lambda_2 = 283, \quad \lambda_2 = -63.$$

The sum of the weighted squared residuals for the positive $\lambda_1$ set is smaller but both sets are good fits (50% of repeats would be worse). The sum of the weighted squared residuals is strictly speaking not $\chi^2$, because we have not taken into account the correlation in some of the experimental values, e.g. $\alpha_K$ and $K/L_1$.

In cases of large penetration effect, Hager and Seltzer indicate that the next higher order $E1$ penetration parameter $\lambda_3$ may be significant and do give the additional coefficients ($A_6$ and $A_7$) necessary for the analysis of $K$ and $L$ shells only. A weighted least-squares adjustment excluding the $M$-shell data yields, again for negligible $M2$ contribution,

$$\lambda_1 = 16.3, \quad \lambda_1 = -20.1,$$

$$\lambda_2 = -272, \quad \lambda_2 = -548,$$

$$\lambda_3 = -9.4, \quad \lambda_3 = -5.9.$$

Residuals indicate these sets are not significantly better fits than the two parameter sets.

We have also allowed the $M2$ fraction, $Q$, to be a free parameter along with $\lambda_1$ and $\lambda_2$ in a weighted least-squares minimization (no magnetic penetration considered) but this produced sets in which $Q$ was negative, whereas physically $0 \leq Q \leq 1$. This result does imply that the $M2$ component probably is much smaller than the ~50% allowed by our $L_3$ conversion limit.

In summary for the 265.9 keV $E1$ transition we find the anomalous conversion data adequately explained with $E1$ penetration; two separate regions of the $(\lambda_1, \lambda_2)$ plane appear equally good as far as the internal conversion data are concerned. No $M2$ contribution is required but on the basis of our $L_3$ conversion limit we cannot rule it out below the 50% level. Certainly the observation of the actual $L_3$ intensity would be an important addition to the information.

Not much can be said about the expected anomalous conversions in the 298 keV transition on the basis of only observed $K$ conversion (Table II). Its $K$-conversion coefficient, 0.30, lies between the $E1$ value, 0.0340, and the $M2$ value, 3.15, and thus can be explained by $E1$-$M2$ mixing. Comparing these $K$-shell values to those of Table V for the analogous 266 keV case, one sees that if penetration conversion indeed contributes significantly to the 298 keV case, it generates an anomaly factor far smaller than in the 266 keV conversion, i.e., $[\alpha_K(\text{expt})/\alpha_K\text{theo.}]_{E1}$, ~10 for the 298 keV case, compared to ~100 in the 266 keV case.

### 2. 471.8 keV M1 anomaly

Turning now to the 471.8 keV transition, one finds that neither internal conversion coefficients nor relative shell conversion intensities of the 471.8 keV transition can be explained with simple $M1+E2$ mixing. Figure 7 shows the $L$-subshell conversion lines for the 472 keV transition. Table VI gives the relevant experimental numbers and the theoretical values of Hager and Seltzer[26] which have been used in the analysis (Ref. 26 also lists the references for $N, O$, and $P$ shell ICC used for Table II). While most of the values fall within the

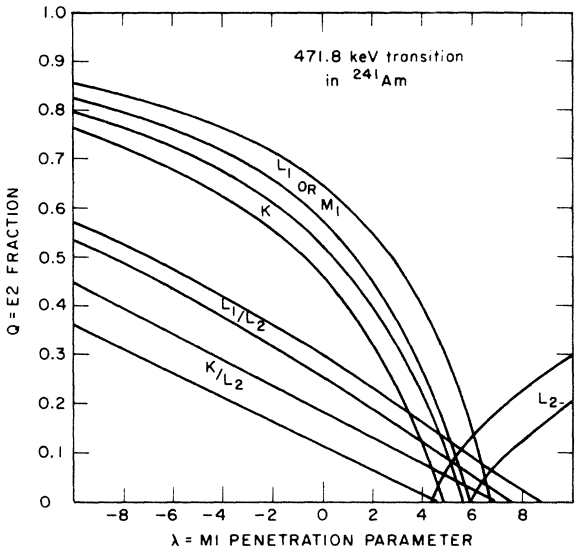


FIG. 9. $M1$ penetration plus $E2$ mixing analysis of the internal conversion of the 471.8 keV transition in $^{241}$Am. Each experimental value (with its uncertainty) for an internal conversion coefficient (ICC) or for an ICC ratio generates a band in the $(Q, \lambda)$ plane [see text, Eq. (2)]. The $L_1$ and $M_1$ bands are very nearly the same. The $M_2$ band is very broad and is not shown but it includes the region near $Q = 0.07$, $\lambda = 5.5$. For $\lambda = 0$ (no penetration) the $E2$ fractions predicted by the several experimental quantities are not consistent with each other (the $L_2$ ICC is not even in the $E2 + M1$ range). The region of $Q = 0.07$ and $\lambda = 5.5$ produces better agreement, although no common area exists for these (± one standard deviation) bands. Other regions of the $Q$, $\lambda$ plane ($0 \leq Q \leq 1$) have no better fit.

$M1+E2$ range they give inconsistent $E2$ fractions. Note the $L_2$ ICC is outside the $M1+E2$ range, being smaller than the $M1$ value, as also is the $M_2$ ICC, but with an uncertainty bringing it into the range.

An analysis taking into account penetration effects in the $M1$ internal conversion calculations is exhibited in Fig. 9. In this discussion $Q$ is the $E2$ fraction, and first we neglect $E2$ penetration effects. For the 471.8 keV transition we have no independent knowledge of the $E2+M1$ mixing so both $Q$ and $\lambda$ are regarded as free parameters. Each experimental value with its uncertainty generates a band in the $(Q, \lambda)$ plane.

The unsatisfactory nature of the multipole mixing analysis with no penetration can be seen in Fig. 9 by noting that at $\lambda = 0$ the $E2$ fractions predicted by the various experimental quantities are disparate and the $L_2$ band does not even cross the $\lambda = 0$ line.

While it is clear from Fig. 9 that a value of $\lambda$ between 5 and 6 and an $E2$ fraction of less than 0.1 improves the situation, there is actually no common overlap of the bands which are generated by one standard deviation; two standard deviations would clearly generate a common area. A weighted least-squares adjustment of $Q$ and $\lambda$ using the 8 quantities of Table VI yields $Q = 0.07$, $\lambda = 5.5$. The sum of the weighted squared residuals indicates that the fit is not excellent (only 10% of repeats would be worse) as we already saw from Fig. 9. In order to see if any better fit could be obtained, the $E2$ penetration of expression (1) was introduced and a four parameter weighted least-squares adjustment was made using the 8 quantities of Table VI. This yielded

$$Q = 0.008,$$
$$\lambda = 5.9,$$
$$\lambda_1 = 62,$$
$$\lambda_2 = -1.0\times 10^3,$$

with very little improvement in the sum of the squares of the residuals compared to the fit with only $M1$ penetration. We note in addition that the 430 keV (pure $E2$) transition from the 471.8 keV level to the $\frac{7}{2}$ member of the ground-state band shows no large anomalies; hence, the existence of large $E2$ penetration [$\lambda_1$ and $\lambda_2$ found above increase ordinary $\alpha(E2)$ ~ threefold] for transitions between these Nilsson states appears not realistic.

In summary, we regard the 471.8 keV transition as an anomalous $M1$ transition with $E2$ fraction of <10% and with $M1$ penetration parameter defined in (2) having a value between 5 and 6. We have no evidence for any $E2$ penetration. The fact that the analysis was not successful within the bands generated by one standard deviation is disturbing and indicates additional experimental work on this transition might be well spent.

This transition has been listed by Krpić and Aničin[30] as one which lends itself to a determination of the ratio of the effective spin gyromagnetic ratio, $g_{s,\mathrm{eff}}$ of the bound odd nucleon to that of the free nucleon, $g_{s,\mathrm{free}}$. Using their analysis and our value for $\lambda$, one finds

$$\eta = \frac{g_{s,\mathrm{eff}}}{g_{s,\mathrm{free}}} > 0.95 .$$

This value is larger than analyses[31] for odd mass deformed nuclei with $A = 150$–$186$ which give $\eta = 0.6$–$0.7$.

As noted above, anomalous conversion is also expected in the 463.3 and 504.4 keV analogous $M1+E2$ transitions. Although in Table II they are analyzed satisfactorily as $M1+E2$ admixtures with quite high $E2$ components on the basis of the available $K$ and $L_1$ (for the 463.3 keV case) conversions, they are both quite probably cases of anomalous $M1$ conversion with much smaller $E2$ components. The ratios of their $K$ (and $L_1$) conversion coefficients to the theoretical $M1$ coefficients are very close to the same ratios for the 471.8 keV transition.

### 3. *Retardation of anomalous M1 and E1 transitions*

Asaro *et al.*[20] have found a correlation between the $E1$ anomaly factor and the $\gamma$-ray retardation over single-particle estimate. From their graph an anomaly factor of ~100 for the 266 keV transition corresponds to a retardation factor of $2\times 10^7$. The $E1$ single-particle half-life[32] retarded by this factor gives a partial half-life of $1\times 10^{-7}$ sec. The $M2$ single-particle half-life is also $1\times 10^{-7}$ sec which, if unretarded, is consistent with our upper limit of 50% $M2$. The over-all half-life for 266 keV photon emission will then lie in the range $(0.5-1)\times 10^{-7}$ sec depending on $M2$ retardation, and, from the photon ratios of Table I, the 471.8 keV transition from the same level has then a photon emission half-life of $3$–$6\times 10^{-10}$ sec. The single-particle photon half-lives of the 471.8 keV transition are $1.3\times 10^{-10}$ sec ($E2$) and $2.3\times 10^{-13}$ sec ($M1$). From these and our upper limit of 10% $E2$ admixture in the 471.8 keV transition, coupled with the assumption[28] of no $E2$ retardation we obtain a retardation factor for the $M1$ component of $4$–$8\times 10^3$, associated with the principal source of the anomalous conversion.

### 4. *K internal conversion near threshold*

We find that the $K$ internal conversion coefficients of the 132, 165, and 180 keV mainly $M1$

(+$E2$) transitions are lower than the theoretical values of Hager and Seltzer[25] by 30, 15, and 7%, respectively. (The $K$ conversion electron of the 132 keV transition is at 7 keV.) We have observed a similarly low value in the 140.7 keV $M1$ transition in $^{250}$Cf ($E_{e^-}$ = 5 keV). Consideration of the possibility of missed electron intensity in degraded very low intensity line tails of these near-$K$-threshold transitions indicates that such missing intensity on other low energy conversion lines would seriously distort some intensity balances in the decay scheme that are satisfactory as here given.

Further, such added tail intensity on the 32 keV $L$, $M$, and $N$ lines would destroy the good consistency of the 98.5% $M_1$ + 1.5% $E2$ mixing character obtained from the absolute $\alpha_{L_1}$, $\alpha_{M_1}$, and $\alpha_{N_1}$ conversion coefficients with that derived from the $L$, $M$, and $N$ subshell ratios (Table II). We have also obtained agreement with the theoretical $M1$ $K$-conversion coefficient of the 14 keV transition in $^{57}$Fe, at a similar low electron energy, 7 keV, with a similarly deposited source (retarded isotope separator beam). These observations suggest that near $K$-threshold $M1$ ICC for very heavy elements are deserving of more careful investigation, experimentally and perhaps also theoretically. For a somewhat lighter isotope, $^{164}$Ho, however, the $K$-conversion coefficient for a 56.64 keV $M1$ transition, only 1 keV above threshold, was measured[33] as 12.3 ± 0.5, compared to the theoretical value of 11.7.

### 5. $P_1$-shell conversion coefficients

Figure 10 shows some examples of outer shell conversion lines for the 15.228, 32.639, and 132.413 keV transitions, to illustrate the basis for our assignment of $P_1$ line intensities. We find that the experimental $P_1$ subshell conversion coefficients for $M1$ transitions are about twice the theoretical values.[26] The latter include finite nuclear size and screening corrections. The ratios of experimental to theoretical $M_1/P_1$, $N_1/P_1$, and $O_1/P_1$ ratios, given in Table VII, show this disparity in

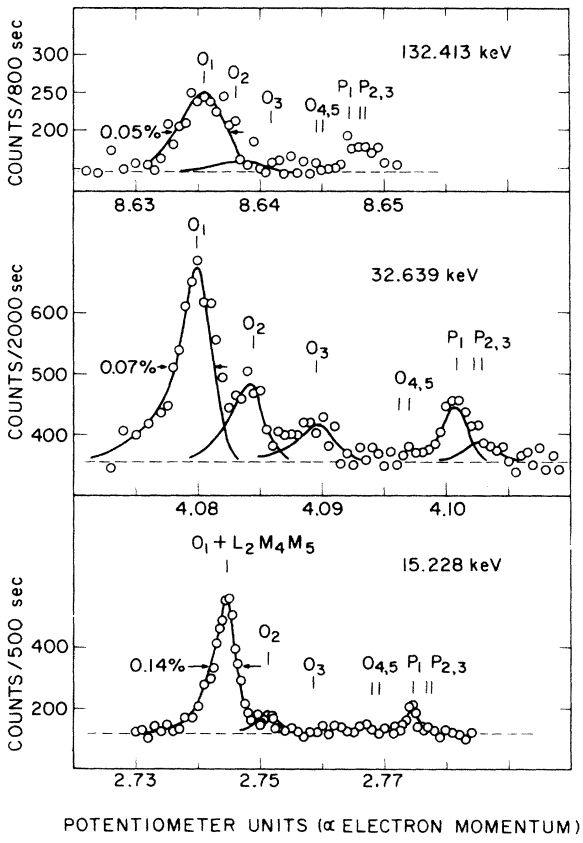


FIG. 10. Outer shell conversion for three transitions in $^{241}$Am. The vertical marks with shell labels are positions calculated for the line peaks using the indicated transition energy and americium binding energies. In the 15.228 and 32.639 keV cases it is clear that the $P$ lines are predominantly $P_1$ both from the expected subshell intensities for these ~99% $M1$ transitions (as in the $O$ subshell intensities), and from the mismatch with the $P_{2,3}$ binding energies (interpolated from experimental values at $Z$ = 92, 98, 100). The $P_1$ to $P_2$ spacing is ~20 eV. We have assigned all the intensity in the $P$ line to $P_1$ in the 132.413 keV case from other subshell intensity data even though the position (statistically uncertain) appears to indicate possible $P_{2,3}$ contribution.

TABLE VII. Comparison of $P_1$ and $O_1$ internal conversion coefficients (ICC) in $^{241}$Am to theory [see O. Dragoun, Z. Plajner, and F. Schmutzler (Ref. 26)].

| Transition (keV) | Ratios used | $P_1$ ICC exp./theo. | Ratios used | $O_1$ ICC exp./theo. |
|---|---|---|---|---|
| 15.23 | $M_1/P_1$ | 2.5 ± 0.3 | | |
| 32.64 | $M_1/P_1$, $N_1/P_1$, $O_1/P_1$ | 1.8 ± 0.3 | $M_1/O_1$, $N_1/O_1$ | 0.99 ± 0.08 |
| 132.41 | $M_1/P_1$, $N_1/P_1$, $O_1/P_1$ | 2.2 ± 0.8 | $M_1/O_1$, $N_1/O_1$ | 1.15 ± 0.13 |
| | Ave. | 2.2 ± 0.3 | | |
| 165.0 | | | $M_1/O_1$, $N_1/O_1$ | 1.4 ± 0.4 |
| | | | Ave. | 1.04 ± 0.07 |

the $P_1$ calculations for the above three transitions. From the similar ratios of the $M_1/O_1$ and $N_1/O_1$ ratios for the 32.6, 132.4, and 165.0 keV transitions in Table VII one sees that the $O_1$ subshell conversion coefficients are in agreement with the experimental values. The $O_1$ of the 15.2 keV transition was not resolved from the $L_2M_4M_5$ intense Auger line, so it could not be evaluated for this comparison. Figure 11 shows that low energy conversion lines in the $L$-Auger region can generally be distinguished from the Auger lines at this high resolution because of the larger width of the latter arising at least partly from the summed natural width contributions of the three subshells involved. The $M_3$ line of the 15.2 keV transition is only slightly wider than the 0.05% instrumental resolution, whereas the main Auger lines are over twice as wide.

## V. $K$-AUGER TRANSITIONS AND FLUORESCENT YIELD

We have measured seven of the nine possible $KLL$- and two $KLM$-Auger electron lines. The $KLL$ lines are shown in Fig. 12, and the $K$ Auger energies and intensities are given in Table VIII, along with the intensities of the $KLL$-Auger lines observed by Ewan *et al.*[34] in $_{94}$Pu at about the same resolution, but with smaller statistical uncertainty. The energy predictions for both Am and Pu $KLL$-Auger lines[35] are given for comparison; these we have recalculated with more accurate shell binding energies than those used by Shirley.[35] The differences of the experimental and calculated energies are given in columns 4 (Am) and 12 (Pu).

Comparison of the relative intensities of the Am and Pu $K$-Auger lines indicates that all the lines except the two $KL_3L_3$ are in agreement within assigned errors, and are thus probably assigned on a consistent basis for the two elements.

The Pu intensities, with the satellite and main Auger intensities summed, are in excellent agreement with the $j$-$j$ coupling relativistic Hartree-Fock-Slater calculations of Bhalla and Ramsdale[36] as are all the Am Augers except the $KL_3L_3$. The correctness of the assignments of all but the $KL_3L_3$ lines in Am and in Pu is further supported by the fairly equal values (column 5 vs column 13) of the differences of each value in column 4 or column 12 from the first ($KL_1L_1$) value in that column. That the column 4 (and 12) differences of experimental and calculated Auger energies disagree absolutely by ~75 eV may originate in a relative calibration

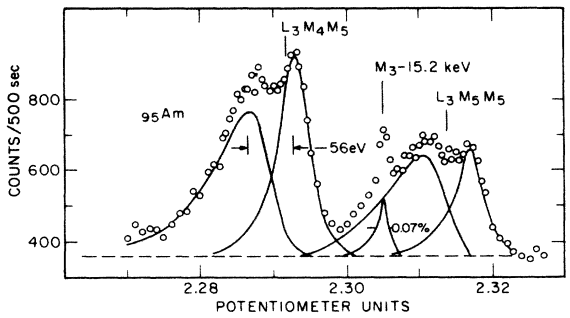


FIG. 11. $M_3$ conversion line of the 15.228 keV transition showing that it is not difficult to distinguish the narrower conversion lines in the complex $L$-Auger spectrum. These $L_3MM$ lines in particular have broadened intense low energy satellites arising from that large fraction of the $L_3$ initial hole states that result from Coster-Kronig transitions following initial $L_1$ and $L_2$ vacancies so that the $L_3MM$-Auger transition takes place with an additional ("spectator") vacancy in an outer shell and with attendant energy shift (56 eV) to lower energy. Marks show calculated Auger line positions.

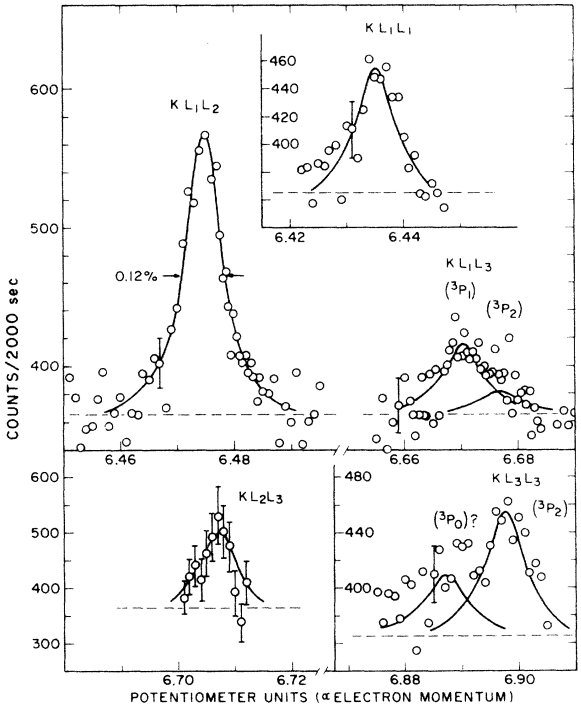


FIG. 12. $KLL$-Auger lines of americium. These very weak lines were examined late in the experiment and are decay corrected to a common late time. All the sketched line shapes are the same as $KL_1L_2$, whose width, because of the $K$-shell natural width is ~2 times an $L$, $M$, etc. line of this same energy. The relatively intense and well separated (250 eV) $KL_3L_3(^3P_0)$ satellite is not supported by other (much better statistically, Ref. 34) observations at $Z=94$ and is probably an unassigned conversion line. The main $KL_3L_3(^3P_2)$ line probably also contains an unresolved conversion line component which accounts for ~$\frac{1}{2}$ its intensity.

TABLE VIII. $K$-Auger electrons in $^{241}$Am following electron capture in $^{241}$Cm: comparison to Auger electrons in Pu [a] and to theory.

| 1 | $^{241}$Am 2 | 3 | 4 | 5 | 6 | 7 | 8 | Pu 9 | 10 | 11 | 12 | 13 |
|---|---|---|---|---|---|---|---|---|---|---|---|---|
| | | | | | Exp. | | Theo. [b] | Exp. | | | | |
| | Energy [keV ± (eV)] | | Col. 2 − col. 3 | Col. 4 − 14 eV | Intensity | | | | Energy [keV ± (eV)] | | Col. 10 − col. 11 | Col. 12 +62 eV |
| Transition | Exp. | Calc. [c] | (eV) [d] | (eV) [d] | %/Cm decay | Rel. to $KL_1L_1$ | | | Exp. | Calc. [c] | (eV) [d] | (eV) [d] |
| $KL_1L_1$ | 77.012(23) | 76.998 | 14 ± 23 | 0 ± 23 | 0.24 ± 0.03 | 1 | 1 | 1 | 75.18(15) | 75.242 | −62 ± 15 | 0 ± 15 |
| $KL_1L_2(^1P_1)$ | 77.895(12) | 77.865 | 30 ± 12 | 16 ± 12 | 0.50 ± 0.06 | 2.1 ± 0.3 | 1.92 | 1.86 ± 0.1 | 76.05(15) | 76.085 | −35 ± 15 | 27 ± 15 |
| $KL_1L_2(^3P_0)$ | ··· | 77.915 | | | | ··· | | ··· | ··· | 76.135 | | |
| $KL_1L_3(^3P_1)$ | 82.32(50) | 82.260 | 60 ± 50 | 46 ± 50 | 0.13 ± 0.04 | 0.54 ± 0.16 | 0.66 | 0.60 ± 0.06 | 80.24(15) | 80.251 | −11 ± 15 | 51 ± 15 |
| $KL_1L_3(^3P_2)$ | 82.47(50) | 82.357 | 113 ± 50 | 99 ± 50 | 0.05 ± 0.02 | 0.21 ± 0.1 | | 0.05 ± 0.03 | 80.40(60) | 80.347 | 53 ± 60 | 115 ± 60 |
| $KL_2L_2$ | Not run | 78.699 | | | | | 0.07 | 0.11 ± 0.04 | 76.78(40) | 76.895 | −115 ± 40 | −53 ± 40 |
| $KL_2L_3$ | 83.169(12) | 83.149 | 20 ± 12 | 6 ± 12 | 0.36 ± 0.12 | 1.5 ± 0.5 | 1.02 | 1.11 ± 0.07 | 81.06(15) | 81.116 | −56 ± 15 | 6 ± 15 |
| $KL_3L_3(^3P_0)$ | 87.36(50) | 87.541 | −181 ± 50 | −195 ± 50 | 0.10 ± 0.05 | 0.4 ± 0.2 | 0.40 | ··· | ··· | 85.278 | | |
| $KL_3L_3(^3P_2)$ | 87.602(24) | 87.609 | −7 ± 24 | −21 ± 24 | 0.20 ± 0.04 | 0.87 ± 0.2 | | 0.40 ± 0.05 | 85.30(15) | 85.345 | −45 ± 15 | 17 ± 15 |
| $KL_1M_1$ | 94.84(50) | | | | 0.13 ± 0.04 | 0.54 ± 0.17 | 0.41 [e] | | | | | |
| $KL_1M_2$ | 95.29(50) | | | | 0.18 ± 0.05 | 0.75 ± 0.21 | 0.41 [e] | | | | | |

[a] G. T. Ewan, J. S. Geiger, R. L. Graham, and D. R. MacKenzie, Can. J. Phys. 37, 174 (1959).

[b] C. P. Bhalla and D. J. Ramsdale, Z. Phys. 239, 95 (1970). These $j$-$j$ coupling calculations sum the contributions of the intermediate coupling satellites into each main line.

[c] D. A. Shirley, Phys. Rev. A 7, 150 (1973). Recalculated using binding energy values obtained from this work and other transuranic measurements (to be published).

[d] Includes experimental error only. Correlated spectrometer calibration error negligible for Am.

[e] C. P. Bhalla, H. R. Rosner, and D. J. Ramsdale, J. Phys. B 3, 1232 (1970).

uncertainty in either set of line measurements, an uncertainty not included in the stated error. A datum on $(K-L_1)$ conversion line energy differences in Ref. 34 is low by ~40 eV from current best values. Since it was obtained from lines not far above the $K$-Auger region, it indicates that the Pu $K$-Auger energies may be low by some such amount, due perhaps to calibration inaccuracy. However, line energy differences are insensitive to these absolute uncertainties. Shirley's[35] calculations can serve as energy references with respect to this question of correctness of line assignment for neighboring elements, regardless of their absolute disagreements with the experimental values, since they are expected to vary smoothly for the same Auger line from element to element. Apart from the $KL_3L_3(^3P_0)$ line the agreement with Shirley's calculations (column 4) is quite good.

With respect to the two $KL_3L_3$ lines the considerable excess of the Am vs the Pu relative intensities and the disagreement of experimental and calculated energies of the Am $KL_3L_3(^3P_0)$ satellite by ~180 eV compared to an average difference of 38 eV cast doubt on these Am assignments, particularly the $KL_3L_3(^3P_0)$. It may be an unassigned conversion line, with a width too large for consideration as other than from the $K$ shell. The intensity comparison of the $KL_3L_3(^3P_2)$ lines indicates that $\sim\frac{1}{2}$ the Am line may be an unresolved conversion line. The two $KLM$ line intensities are compared to Bhalla's calculations[37] (column 8). Agreement is fair.

We have made a detailed study of the $L$-Auger spectra in this decay, observing about 60 lines. A preliminary report[38] on these and correlated $L$-Auger spectra in Pu, Cf, and Fm has been given, and a detailed report will appear elsewhere. In Fig. 11 two examples are shown of "spectator vacancy" satellites of the $L_3M_4M_5$- and $L_3M_5M_5$-Auger transitions, the broadened low energy wings on the main lines. These are the first resolutions of these satellites in radioactive decay; they have been observed in low energy photoionization induced spectra in light noble gases.[39] The satellites originate from those $L_3$ vacancies populated by Coster-Kronig transitions mainly from initial $L_1$ vacancies from $L_1$ capture and $L_1$ conversion, rather than via $K$ $\alpha_1$ x ray or $L_3$ conversion (weak). The Coster-Kronig transition also generates one of a spectrum of $M$ vacancies which remains as a "spectator" during the $L_3$-Auger transition causing (a spread of) energy shifts to produce the satellite. The main line arises from the $L_3$ vacancies without $M$ spectators.

The $K$ fluorescent yield was determined from the $K$-Auger and x-ray intensities. The $KLL$-Auger intensities were augmented by the $KLY$ and $KXY$ intensities from the ratios $KLY/KLL = 0.6 \pm 0.1$ and $KXY/KLL = 0.1$ obtained from the review of Bambynek *et al.*[40] We calculate a $K$ fluorescent yield $\omega_K = 0.965 \pm 0.004$. For $Z = 92$, the $\omega_K$ value selected by Bambynek *et al.* is $0.976 \pm 0.013$, and at $Z = 98$, our[41] $\omega_K$ value is $0.976 \pm 0.005$.


## ACKNOWLEDGMENTS

The authors wish to thank J. Lerner for the isotope-separator preparation of the $^{241}$Cm samples, R. K. Sjoblom for her assistance in some of the chemical purifications, and the cyclotron crew for several irradiations. Helpful discussions with R. R. Chasman are also acknowledged.


*Work performed under the auspices of the U.S. Atomic Energy Commission.


[1] F. Asaro, F. S. Stephens, S. Amiel, and I. Perlman cited in E. K. Hyde, I. Perlman, and G. T. Seaborg, *The Nuclear Properties of the Heavy Elements* (Prentice-Hall, Englewood Cliffs, N. J., 1964), Vol. II, p. 882.

[2] S. G. Nilsson, K. Dan. Vidensk. Selsk., Mat.-Fys. Medd. 29, No. 16 (1955).

[3] I. Ahmad, Lawrence Radiation Laboratory Report No. UCRL-16888, 1966 (unpublished).

[4] G. R. Choppin, B. G. Harvey, and S. G. Thompson, J. Inorg. Nucl. Chem. 2, 66 (1956).

[5] J. Lerner, Nucl. Instrum. Methods 102, 373 (1972).

[6] A. M. Friedman, I. Ahmad, J. Milsted, and D. W. Engelkemeir, Nucl. Phys. A127, 33 (1969).

[7] R. G. Greenwood, R. C. Helmer, and R. J. Gehrke, Nucl. Instrum. Methods 77, 141 (1970).

[8] G. C. Nelson, B. G. Saunders, and S. I. Salem, Z. Phys. 235, 308 (1970).

[9] M. F. Freedman, F. Wagner, F. T. Porter, J. Terandy, and P. P. Day, Nucl. Instrum. Methods 8, 225 (1960).

[10] F. T. Porter, I. Ahmad, M. S. Freedman, R. F. Barnes, R. K. Sjoblom, F. Wagner, Jr., and P. R. Fields, Phys. Rev. C 5, 1738 (1972).

[11] F. T. Porter, M. S. Freedman, F. Wagner, Jr., and I. S. Sherman, Nucl. Instrum. Methods 39, 35 (1966).

[12] S. A. Baranov, V. M. Shatinskii, and V. M. Kulakov, Yad. Fiz. 10, 110 (1969) [transl.: Sov. J. Nucl. Phys. 10, 632 (1970)].

[13] M. A. Preston, Phys. Rev. 71, 865 (1947).

[14] J. Milsted, private communications.

[15] R. A. Glass, R. J. Carr, and W. M. Gibson, J. Inorg. Nucl. Chem. 13, 181 (1960).

[16] R. Marrus, W. A. Nierenberg, and J. Winocur, Phys. Rev. 120, 1429 (1960).

[17] A. Bohr and B. R. Mottelson, K. Dan. Vidensk. Selsk., Mat.-Fys. Medd. 27, No. 16 (1953).

[18] A. K. Kerman, K. Dan. Vidensk. Selsk., Mat.-Fys. Medd. 30, No. 15 (1955).

[19]J. R. Erskine, G. Kyle, R. R. Chasman, and A. M. Friedman, Phys. Rev. C (to be published).
[20]F. Asaro, F. S. Stephens, J. M. Hollander, and I. Perlman, Phys. Rev. 117, 492 (1960).
[21]T. Yamazaki and J. M. Hollander, Nucl. Phys. 84, 505 (1966).
[22]G. Alaga, Nucl. Phys. 4, 625 (1957).
[23]J. K. Major and L. C. Biedenharn, Rev. Mod. Phys. 26, 321 (1954).
[24]Y. A. Ellis, Nucl. Data B6 (No. 6), 621 (1971).
[25]H. Brysk and M. E. Rose, in *Nuclear Spectroscopy Tables*, edited by A. H. Wapstra, G. J. Nigh, and R. van Lieshout (North-Holland, Amsterdam, 1959), p. 59.
[26]R. S. Hager and E. C. Seltzer, Nucl. Data A4, 1 (1968); for $K$, $L$, $M$ shells with compter-program energy interpolation; O. Dragoun, H. C. Pauli, and F. Schmutzler, Nucl. Data A6, 235 (1969) for $N$ shells; O. Dragoun, Z. Plajner, and F. Schmutzler, Max-Planck-Institut für Kernphysik, Heidelberg Report No. MPIH-1969-V5 (unpublished), for $O$ and $P$ shells. Plotted energy interpolation for $N$, $O$, and $P$ shells gave $\leq 5\%$ errors.
[27]S. G. Nilsson and J. O. Rasmussen, Nucl. Phys. 5, 617 (1958).
[28]E. L. Church and J. Weneser, Annu. Rev. Nucl. Sci. 10, 193 (1960).
[29]R. S. Hager and E. C. Seltzer, Nucl. Data A6, 1 (1969).
[30]D. K. Krpić and I. V. Aničin, Phys. Rev. C 9, 660 (1974).
[31]Z. Bochnacki and S. Ogaza, Nucl. Phys. 69, 186 (1965).
[32]S. A. Moszkowski, in *Alpha-, Beta-, and Gamma-Ray Spectroscopy*, edited by K. Siegbahn (North-Holland, Amsterdam, 1965), Vol. II, p. 881; statistical factor $S$ was taken as unity.
[33]N. Kaffrell and J. Zylicz, in *Proceedings of the International Conference on Inner Shell Ionization Phenomena, Atlanta, 1973*, edited by R. W. Fink *et al.* (U.S. Atomic Energy Commission, 1973), p. 1887, USAEC CONF-720404.
[34]G. T. Ewan, J. S. Geiger, R. L. Graham, and D. R. MacKenzie, Can. J. Phys. 37, 174 (1959).
[35]D. A. Shirley, Phys. Rev. A 7, 1520 (1973).
[36]C. P. Bhalla and D. J. Ramsdale, Z. Phys. 239, 95 (1970).
[37]C. P. Bhalla, H. R. Rosner, and D. J. Ramsdale, J. Phys. B 3, 1232 (1970).
[38]M. S. Freedman and F. T. Porter, in *Proceedings of the International Conference on Inner Shell Ionization Phenomena, Atlanta, 1973*, edited by R. W. Fink *et al.* (U.S. Atomic Energy Commission, 1973), Vol. 1, p. 680, USAEC CONF-720404.
[39]K. Siegbahn, C. Nordling, G. Johansson, J. Hedman, P. F. Hedén, K. Hamrin, U. Gelius, T. Bergmark, L. O. Werme, R. Manne, and Y. Baer, *ESCA Applied to Free Molecules* (North-Holland, Amsterdam, 1969).
[40]W. Bambynek, B. Crasemann, R. W. Fink, H.-U. Freund, H. Mark, C. D. Swift, R. E. Price, and P. V. Rao, Rev. Mod. Phys. 44, 716 (1972).
[41]I. Ahmad, F. T. Porter, M. S. Freedman, R. K. Sjoblom, R. F. Barnes, and P. R. Fields, to be published.